Supporting Information

Amido Rare-Earth (III) and Ca(II) Complexes Coordinated by Tridentate Amidinate Ligand: Synthesis, Structure, and Catalytic Activity in Ring-Opening Polymerization of *rac*-Lactide and *ε*-Caprolactone

Natalia Yu. Rad'kova,[a] Tatyana A. Kovylina,[a] Andrei S. Shavyrin,[a] Anton V. Cherkasov,[a] Georgy K. Fukin,[a] Konstantin A. Lyssenko,[b,c] and Alexander A. Trifonov*[a,b]

Table of contents

*[a]G. A. Razuvaev Institute of Organometallic Chemistry of Russian Academy of Sciences, Tropinina str. 49, 603950 Nizhny Novgorod, GSP-445, Russia
[b]A. N. Nesmeyanov Institute of Organoelement Compounds of Russian Academy of Sciences, Vavilova str.28, 119991 Moscow, GSP-1, Russia. *E-mail:* trif@iomc.ras.ru.
[c]M.V. Lomonosov Moscow State University, Chemistry Department, Leninskie Gory, 119991 Moscow, GSP-1, Russia.

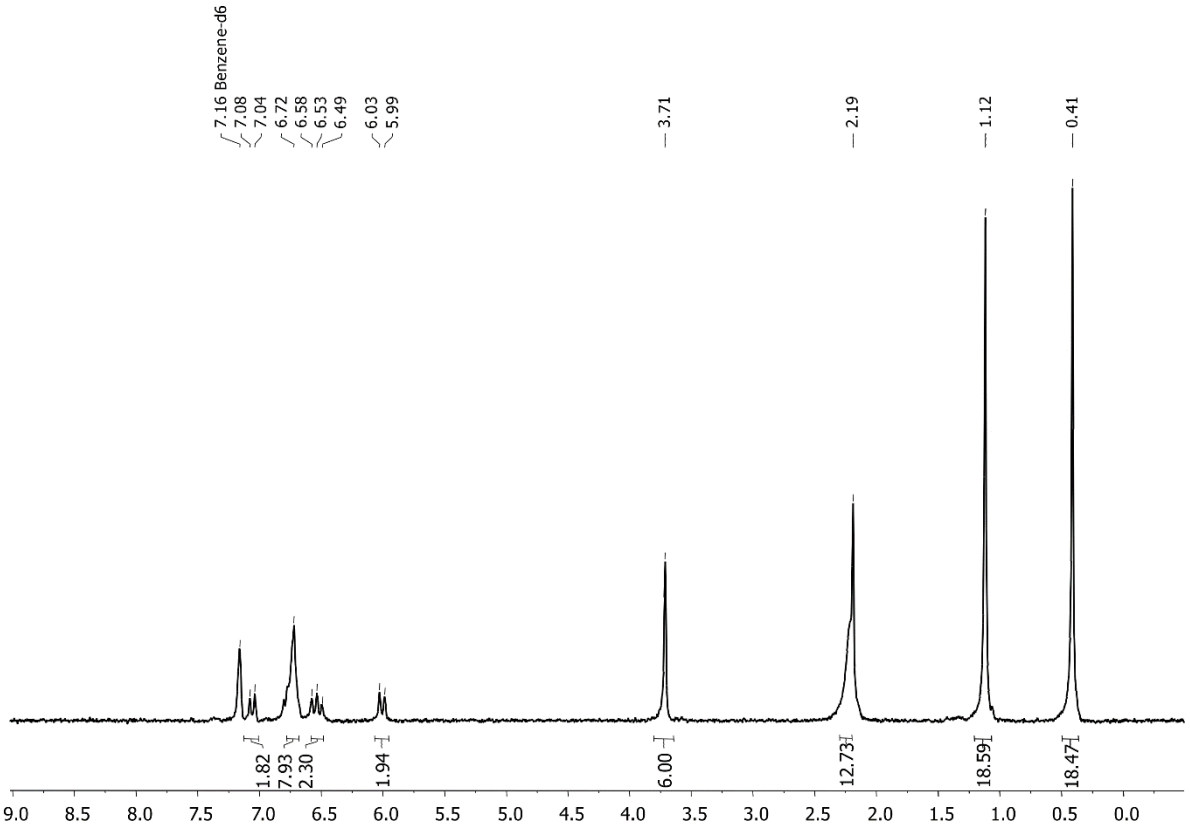

Fig. **S1**. ^{1}H NMR spectrum of [2-MeOC$_6$H$_4$NC(^{t}Bu)N(2,6-Me$_2$C$_6$H$_3$)]$_2$YN(SiMe$_3$)$_2$ (**2**) (200 MHz, C$_6$D$_6$, 298 K).

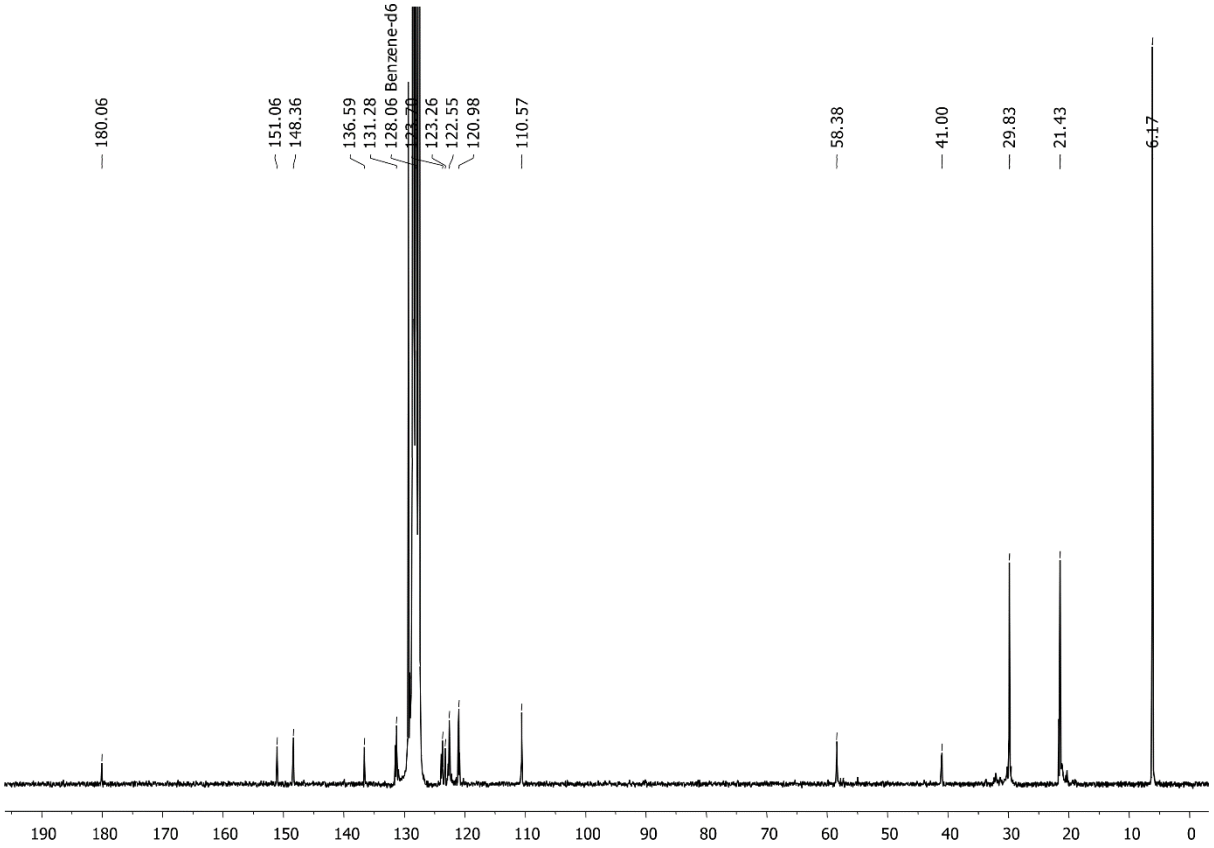

Fig. **S2**. ^{13}C{^{1}H} NMR spectrum of [2-MeOC$_6$H$_4$NC(^{t}Bu)N(2,6-Me$_2$C$_6$H$_3$)]$_2$YN(SiMe$_3$)$_2$ (**2**) (100 MHz, C$_6$D$_6$, 298 K).

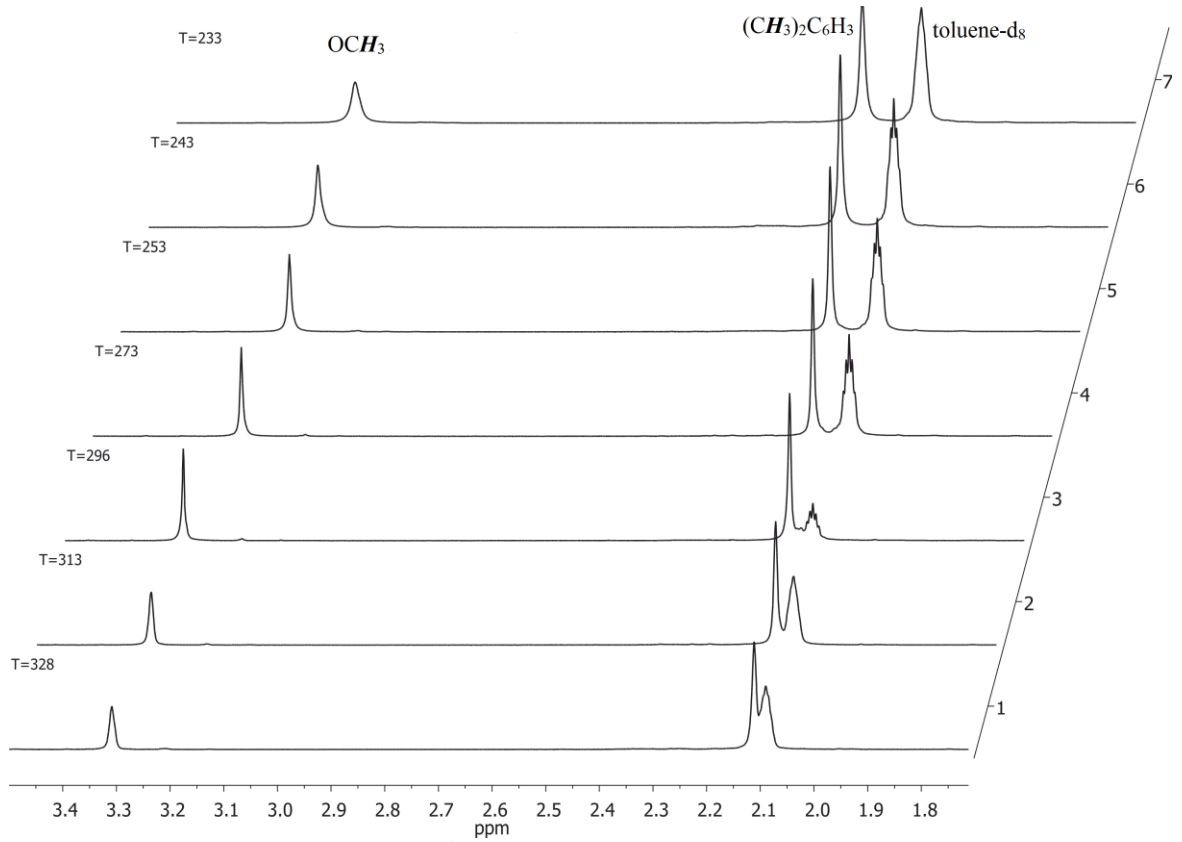

Fig. **S3**. Variable temperature ^{1}H spectra of compound [2-MeOC$_6$H$_4$NC(^{t}Bu)N(2,6-Me$_2$C$_6$H$_3$)]$_2$YN(SiMe$_3$)$_2$ (**2**) (400 MHz, toluene-d$_8$, 233–328 K). Only 2-C*H*$_3$OC$_6$H$_4$ and 2,6-C*H*$_3$C$_6$H$_3$ are shown.

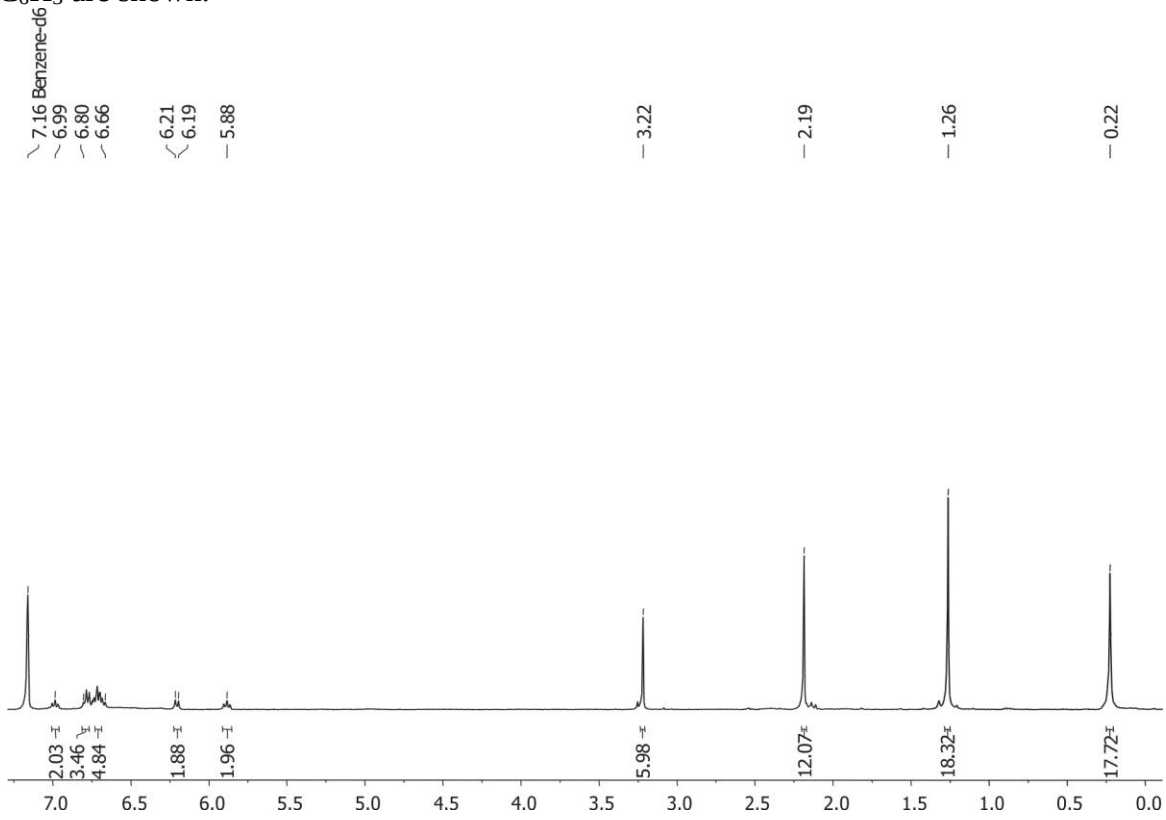

Fig. **S4**. ^{1}H NMR spectrum of [2-MeOC$_6$H$_4$NC(^{t}Bu)N(2,6-Me$_2$C$_6$H$_3$)]$_2$SmN(SiMe$_3$)$_2$ (**3**) (400 MHz, C$_6$D$_6$, 298 K).

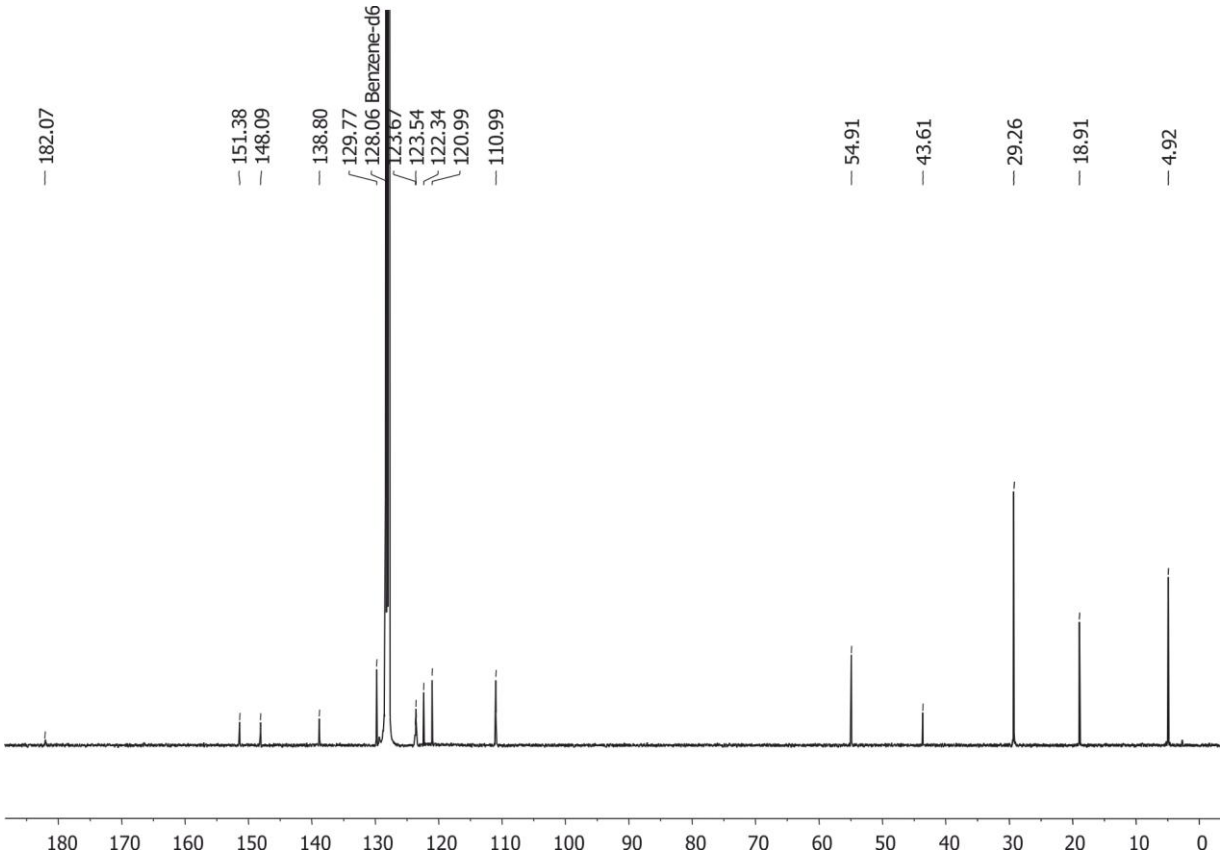

Fig. **S5**. $^{13}C\{^{1}H\}$ NMR spectrum of [2-$MeOC_6H_4NC(^tBu)N(2,6\text{-}Me_2C_6H_3)]_2SmN(SiMe_3)_2$ (**3**) (100 MHz, C_6D_6, 298 K).

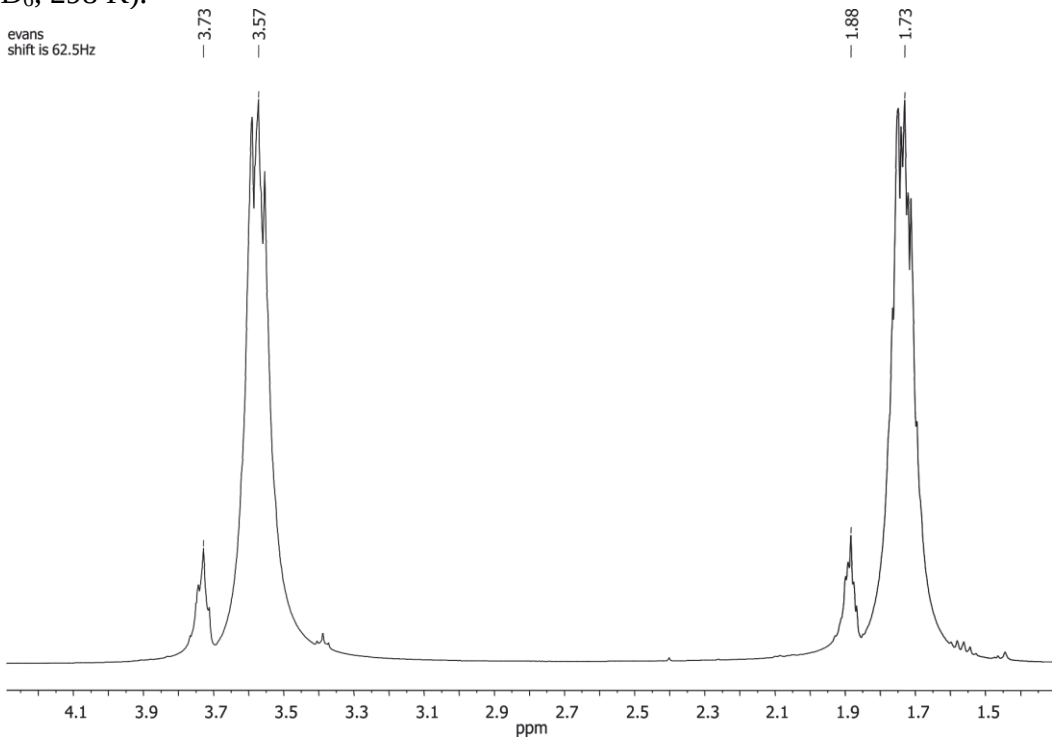

Fig. **S6**. ^{1}H NMR (400 MHz, 298 K, THF) of **3**. Measurement of effective magnetic moment of according to the Evans' method.

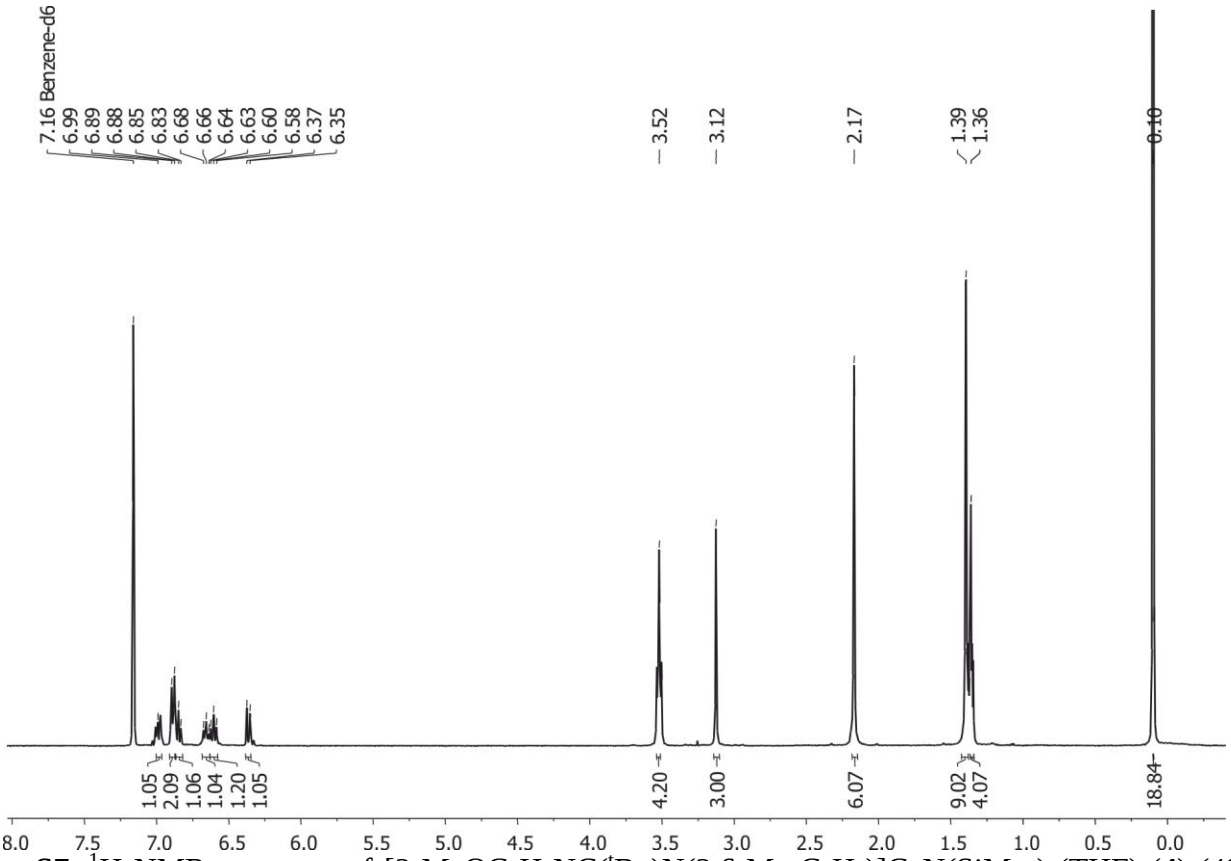

Fig. **S7**. ^{1}H NMR spectrum of [2-MeOC$_6$H$_4$NC(^{t}Bu)N(2,6-Me$_2$C$_6$H$_3$)]CaN(SiMe$_3$)$_2$(THF) (**4**) (400 MHz, C$_6$D$_6$, 298 K).

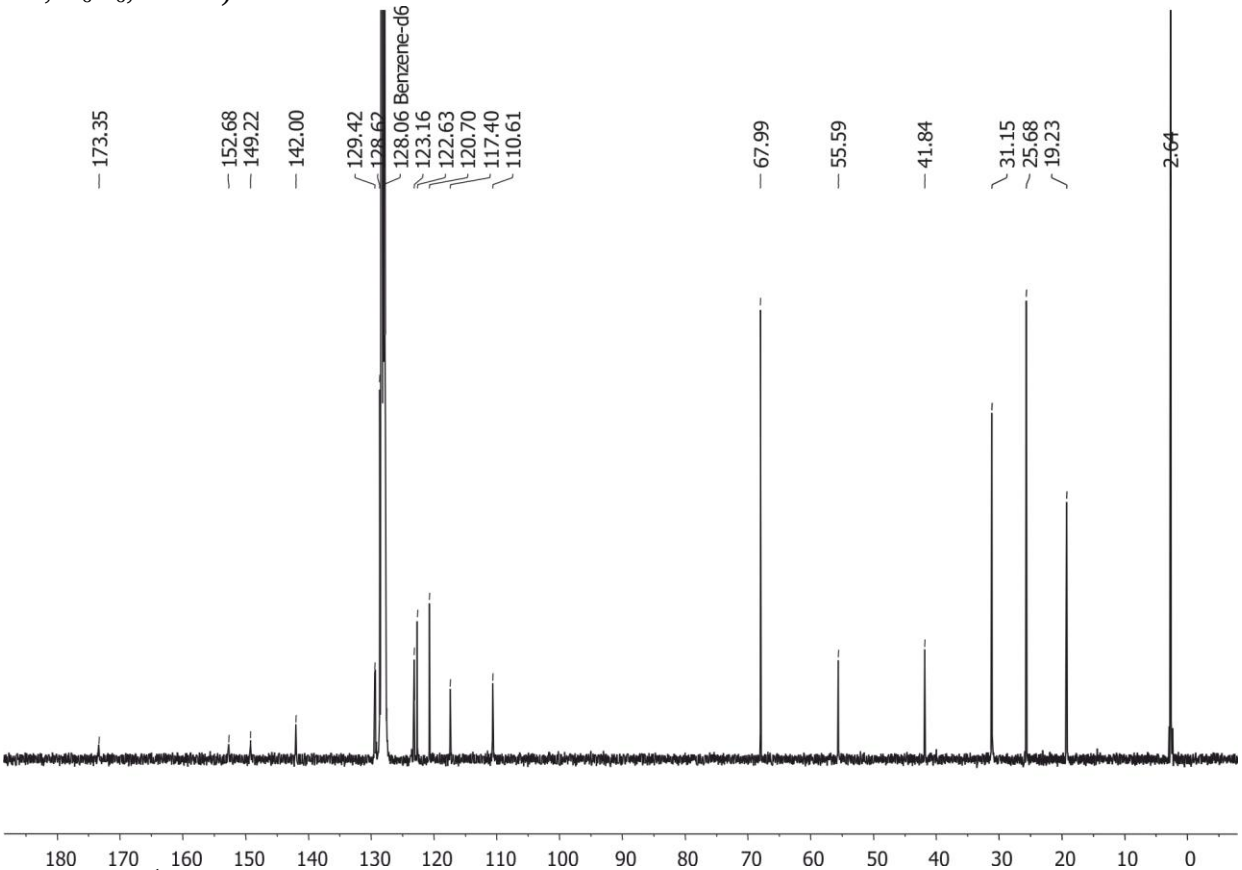

Fig. **S8**. **^{13}**C{^{1}H} NMR spectrum of [2-MeOC$_6$H$_4$NC(^{t}Bu)N(2,6-Me$_2$C$_6$H$_3$)]CaN(SiMe$_3$)$_2$(THF) (**4**) (100 MHz, C$_6$D$_6$, 298 K).

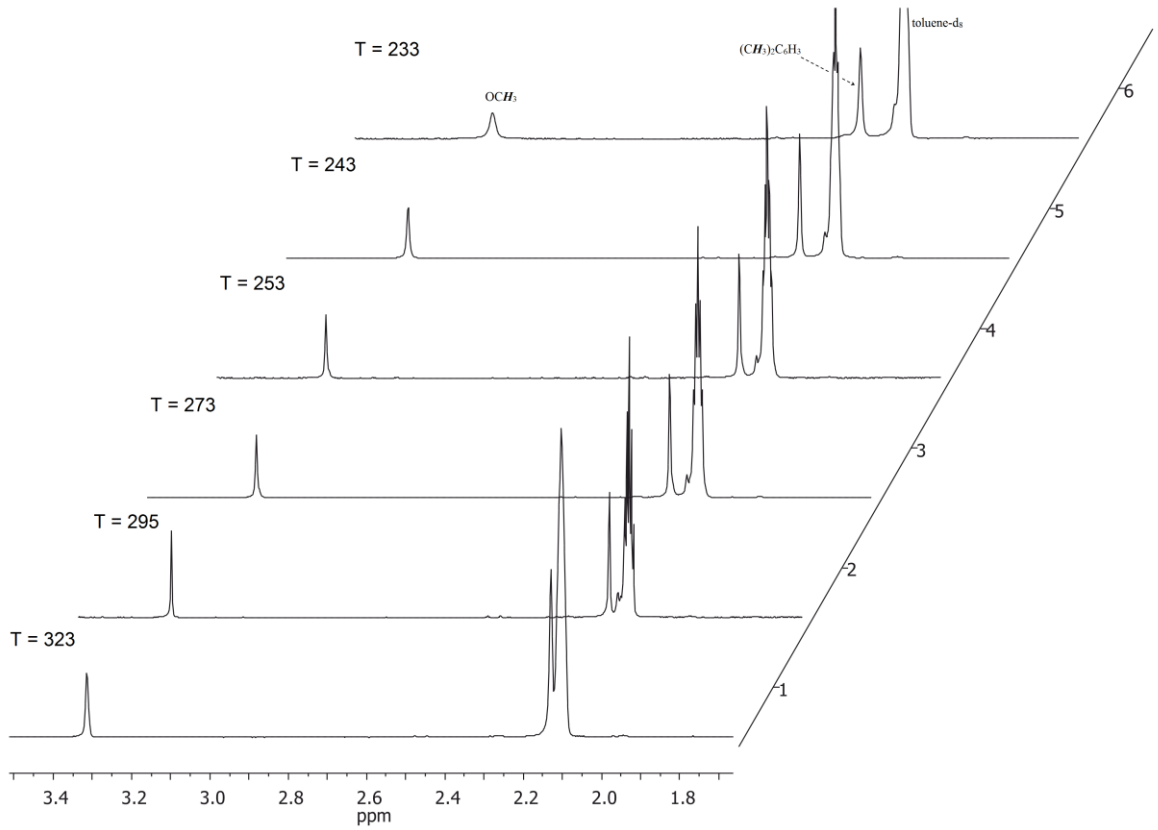

Fig. **S9**. Variable temperature ^{1}H spectra of compound [2-MeOC$_6$H$_4$NC(^{t}Bu)N(2,6-Me$_2$C$_6$H$_3$)]CaN(SiMe$_3$)$_2$(THF) (**4**) (400 MHz, toluene-d$_8$, 233–323 K). Only 2-C*H*$_3$OC$_6$H$_4$ and 2,6-C*H*$_3$C$_6$H$_3$ are shown.

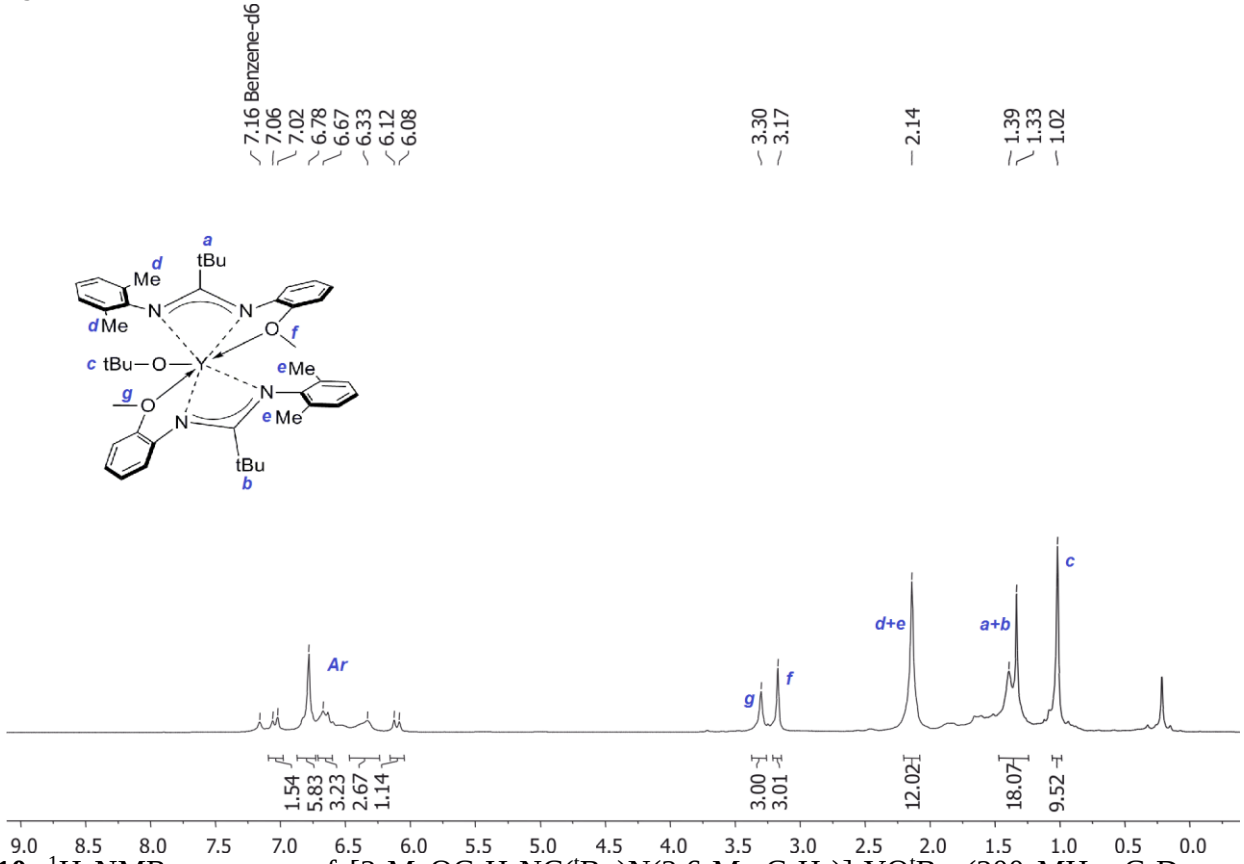

Fig. **S10**. ^{1}H NMR spectrum of [2-MeOC$_6$H$_4$NC(^{t}Bu)N(2,6-Me$_2$C$_6$H$_3$)]$_2$YO^{t}Bu (200 MHz, C$_6$D$_6$, 298 K).

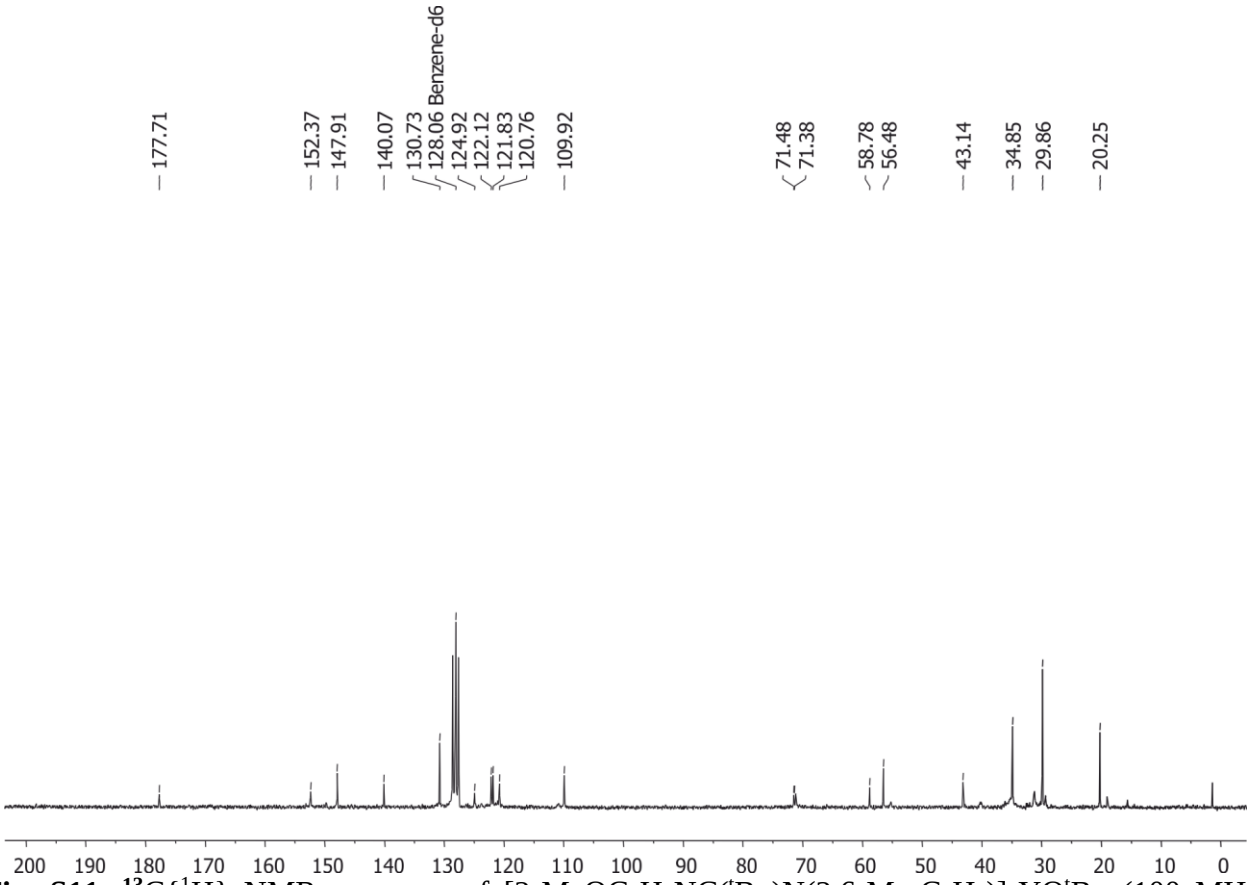

Fig. **S11**. $^{13}C\{^{1}H\}$ NMR spectrum of [2-$MeOC_6H_4NC(^tBu)N(2,6\text{-}Me_2C_6H_3)]_2YO^tBu$ (100 MHz, C_6D_6, 298 K).

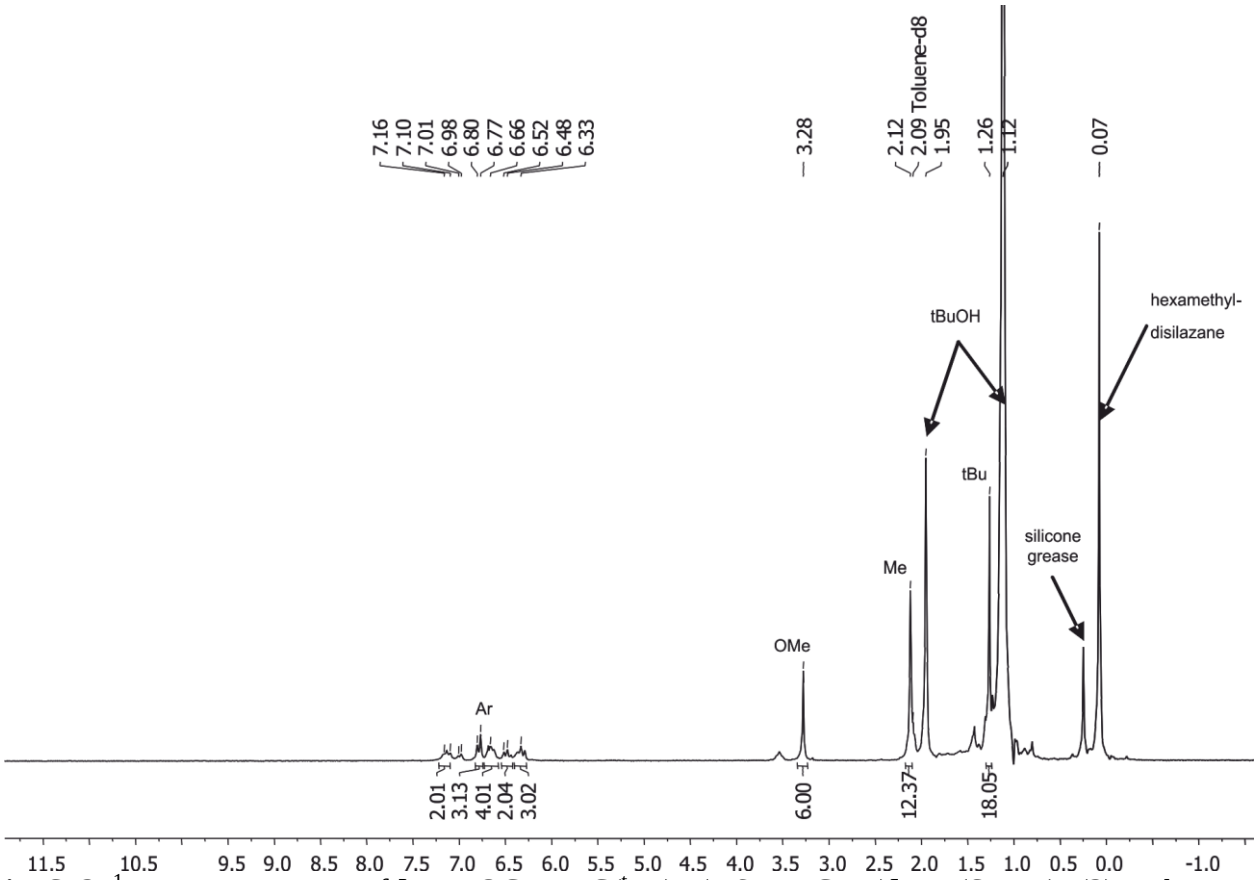

Fig. **S12**. ^{1}H NMR spectrum of [2-$MeOC_6H_4NC(^tBu)N(2,6\text{-}Me_2C_6H_3)]_2YN(SiMe_3)_2$ (**2**) with excess ^tBuOH (200 MHz, toluene-d_8, 298 K).

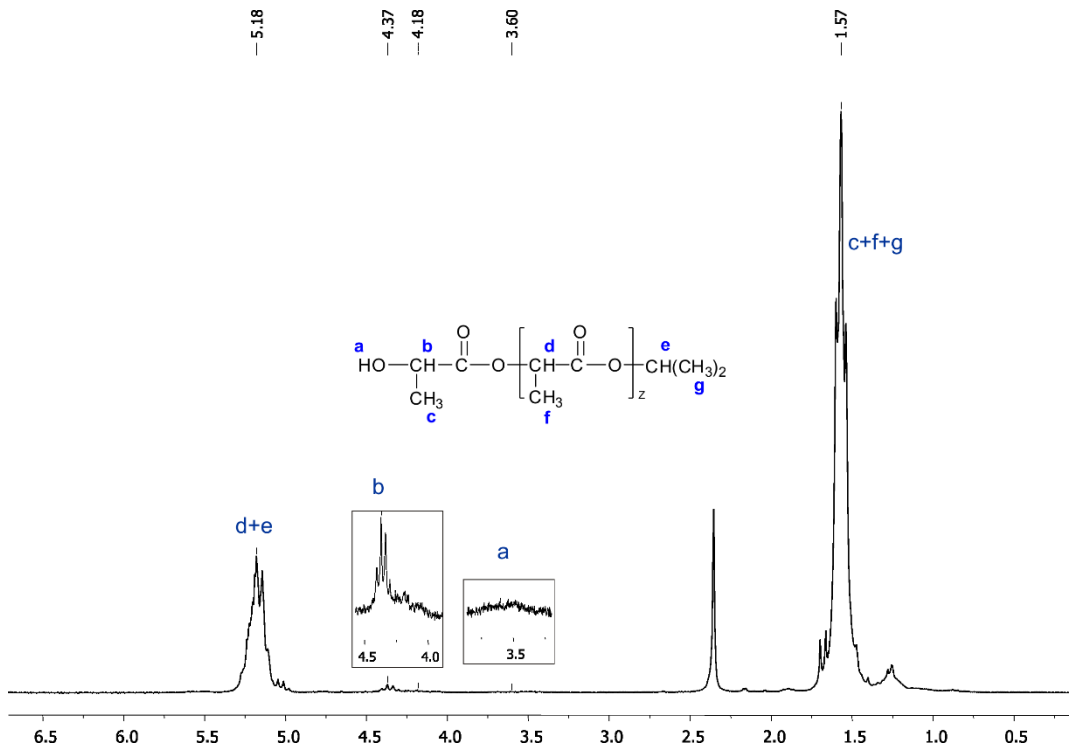

Fig. **S13**. ^{1}H NMR spectrum (200 MHz, $CDCl_3$, 298 K) of PLA obtained in the presence of complex **2**.

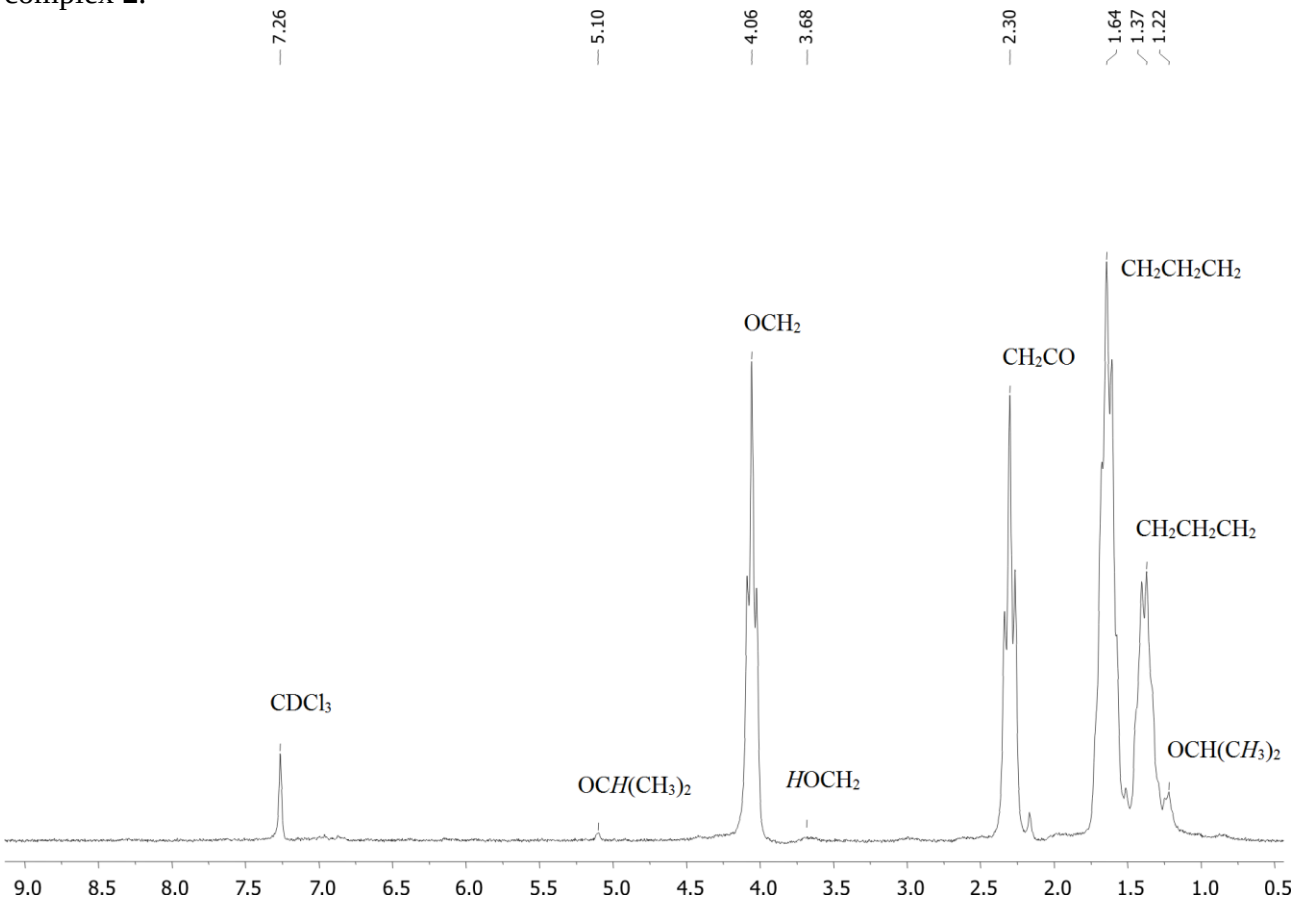

Fig. **S14**. ^{1}H NMR spectrum (200 MHz, $CDCl_3$, 298 K) of PCL obtained in the presence of complex **3**.

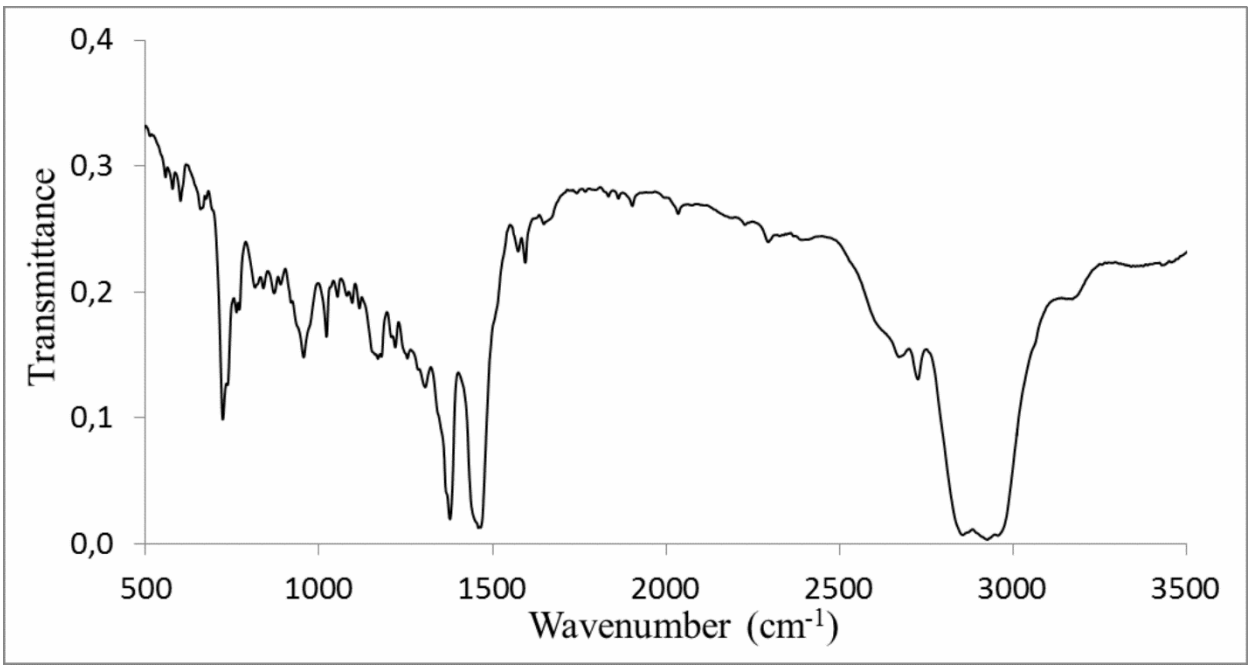

Fig. **S15**. IR spectrum (Nujol, KBr) of complex [2-$MeOC_6H_4NC(^tBu)N(2,6\text{-}Me_2C_6H_3)]_2YN(SiMe_3)_2$ (**2**)

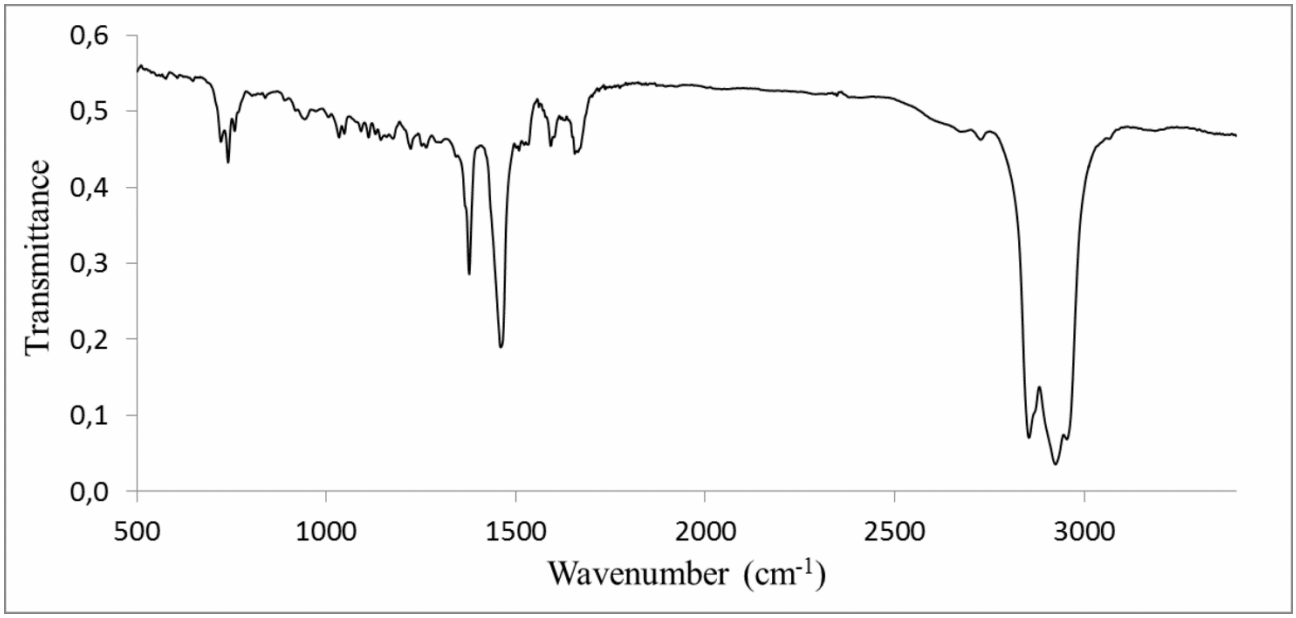

Fig. **S16**. IR spectrum (Nujol, KBr) of complex [2-$MeOC_6H_4NC(^tBu)N(2,6\text{-}Me_2C_6H_3)]_2SmN(SiMe_3)_2$ (**3**)

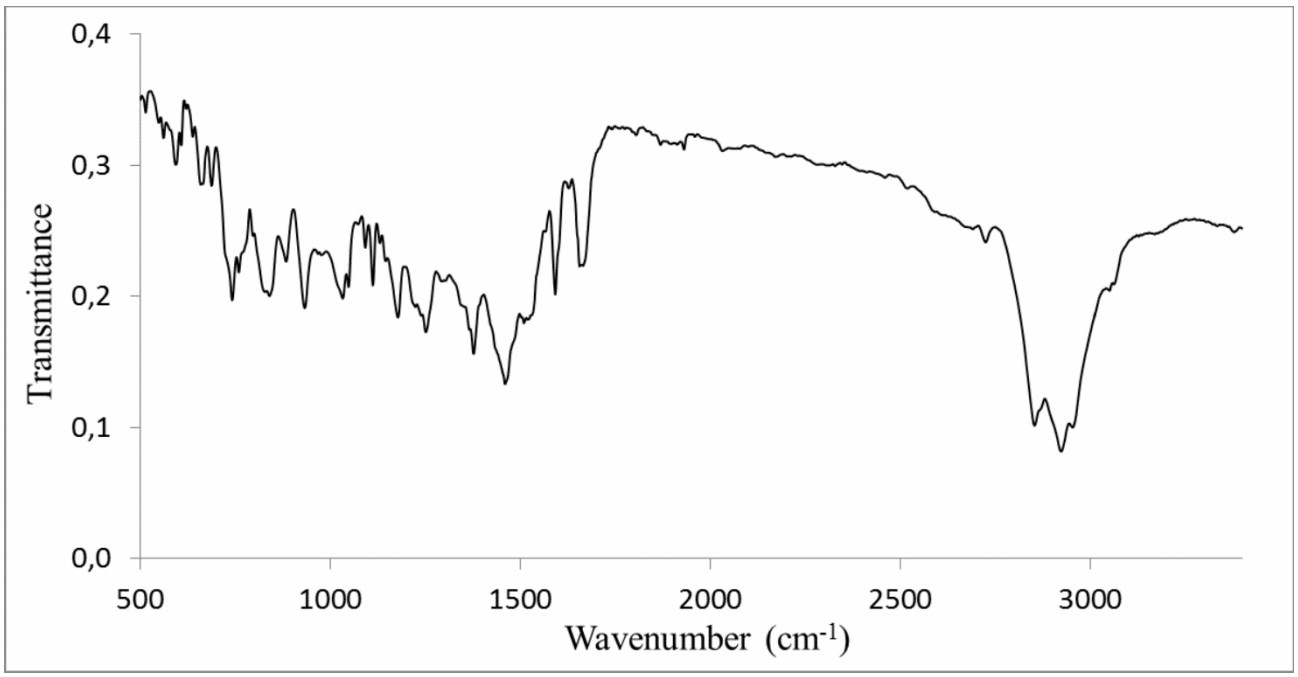

Fig. S17. IR spectrum (Nujol, KBr) of complex [2-MeOC$_6$H$_4$NC(^{t}Bu)N(2,6-Me$_2$C$_6$H$_3$)]CaN(SiMe$_3$)$_2$(THF) (**4**)

Table S1. Crystallographic data and structure refinement details for complexes **1**-**4**

	1	**2**	**3**	**4**
Empirical formula	$C_{20}H_{26}N_2O$	$C_{46}H_{68}YN_5O_2Si_2$	$C_{46}H_{68}SmN_5O_2Si_2$	$C_{30}H_{51}CaN_3O_2Si_2$
Formula weight	310.43	868.14	929.58	581.99
T, K	150	100	120	100
Crystal system	Monoclinic	Monoclinic	Monoclinic	Triclinic
Space group	*P2$_1$/c*	*C2/c*	*C2/c*	*P-1*
a, Å	13.0115(8)	20.9092(9)	20.9858(13)	9.0772(2)
b, Å	17.0106(11)	11.5943(5)	11.6699(7)	9.1571(2)
c, Å	7.8719(5)	20.5513(9)	20.5963(13)	20.5591(5)
α, deg	90	90	90	87.9950(10)
β, deg	93.093(2)	114.9940(10)	114.8950(10)	78.0930(10)
γ, deg	90	90	90	87.9820(10)
V, Å^3	1739.78(19)	4515.6(3)	4575.4(5)	1670.41(7)
Z	4	4	4	2
d_{calc}, g/cm^3	1.185	1.277	1.349	1.157
μ, mm^{-1}	0.073	1.387	1.377	0.289
Crystal size, mm^3	0.40 × 0.33 × 0.28	0.40 × 0.40 × 0.20	0.32 × 0.28 × 0.22	0.34 × 0.25 × 0.12
θ range, deg	1.97–28.74	2.33–30.11	2.05–29.00	2.23–30.05

Reflections collected	12722	48428	44811	40596
Independent reflections	4499	6628	6081	9771
Data / restraints / parameters	4499 / 0 / 218	6628 / 0 / 263	6081 / 0 / 263	9771 / 0 / 378
Final *R* indices [$I > 2\sigma(I)$]	R_1 = 0.0507	R_1 = 0.0261	R_1 = 0.0236	R_1 = 0.0352
	wR_2 = 0.1272	wR_2 = 0.0692	wR_2 = 0.0569	wR_2 = 0.0829
R indices (all data)	R_1 = 0.0636	R_1 = 0.0290	R_1 = 0.0271	R_1 = 0.0526
	wR_2 = 0.1366	wR_2 = 0.0710	wR_2 = 0.0579	wR_2 = 0.0883
$S(F^2)$	1.028	1.045	1.035	1.032
Largest diff. peak, e/Å^3	0.31 / -0.16	0.74 / -0.65	2.45 / -0.63	0.40 / -0.43

Table S2. Selected bond lengths (*d*) and bond angles (ω) in complexes **2** (Y) and **3** (Sm).

Parameter	**2**	**3**	Parameter	**2**	**3**
Bond distance	*d*/Å	*d*/Å	Bond angle	ω/deg	ω/deg
Ln(1)–N(1)	2.358(2)	2.417(2)	N(1)-Ln(1)-N(2)	54.43(3)	53.22(5)
Ln(1)–N(2)	2.4291(9)	2.479(2)	N(2)–C(1)–N(1)	109.50(9)	109.6(2)
Ln(1)–N(3)	2.328(2)	2.380(2)	N(1)-Ln(1)-O(1)	63.05(3)	61.99(5)
Ln(1)–O(1)	2.5325(8)	2.569(2)	C(1)-Ln(1)-N(3)	125.13(2)	125.66(3)
Ln(1)…C(1)	2.901(2)	2.960(2)	C(1)-Ln(1)-C(1A)	109.74(4)	108.69(7)
N(1)–C(1)	1.349(2)	1.351(2)	O(1)-Ln(1)-O(1A)	161.46(4)	163.88(6)
N(2)–C(1)	1.334(2)	1.333(2)			

Table S3. Selected bond lengths (*d*) and bond angles (ω) in complex **4** (Ca).

Parameter	**4**	Parameter	**4**
Bond distance	*d*/Å	Bond angle	ω/deg
Ca(1)−N(1)	2.384(2)	N(1)−Ca(1)−O(1)	66.67(3)
Ca(1)−N(3)	2.302(2)	N(1)−Ca(1)−O(2)	92.66(3)
Ca(1)−O(2)	2.390(2)	O(1)−Ca(1)−O(2)	79.75(3)
Ca(1)−O(1)	2.4178(9)	N(1)−Ca(1)−N(3)	131.50(4)
Ca(1)-C(13)	2.942(2)	O(1)−Ca(1)−N(3)	87.77(3)
Ca(1)-C(14)	2.874(2)	N(1)-Ca(1)…Ar_{centre}	83.6

Ca(1)-C(15)	3.198(2)		
Ca(1)-C(26)	3.159(2)		
N(1)−C(1)	1.364(2)		
N(2)−C(1)	1.309(2)		

Table S4. The percentage of the coordination sphere of the metal atom shielded by the ligands[†] in complexes **2**–**4**.

	2	**3**	**4**
Metal atom	Y	Sm	Ca
G_{sum}	96.0	94.3	86.3
G	93.5	92.4	85.8

G_{sum} – the sum of the solid angles of all ligands coordinated by the metal atom.
G - the percentage of the coordination sphere of the metal atom shielded by the ligands, calculated considering their overlapping.

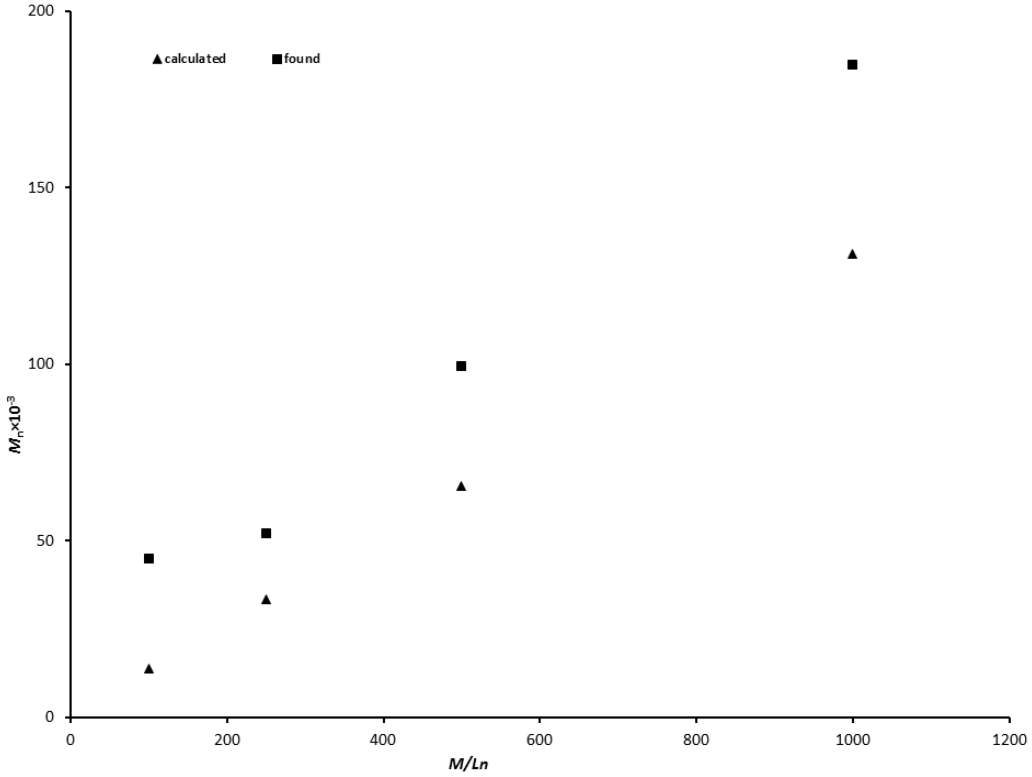

Fig. **S18**. M_n vs $[M]_0/[I]_0$ for ROP of *rac*-LA initiated by **2**. Conditions: toluene, 20 °C, $[M]_0$ = 1.0 mol/L.

[†] I.A. Guzei, M. Wendt, Dalton Trans., 2006, 3991-3999.

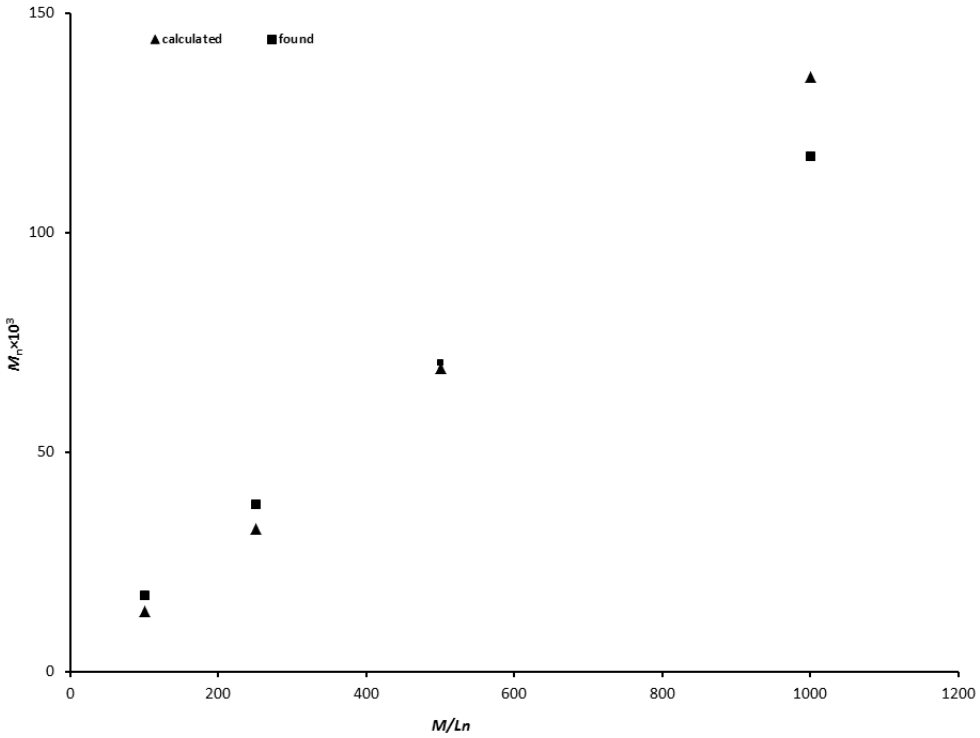

Fig. **S19**. M_n vs $[M]_0/[I]_0$ for ROP of *rac*-LA initiated by **2** in the presence of iPrOH (1 equiv.). Conditions: toluene, 20 °C, $[M]_0$ = 1.0 mol/L.

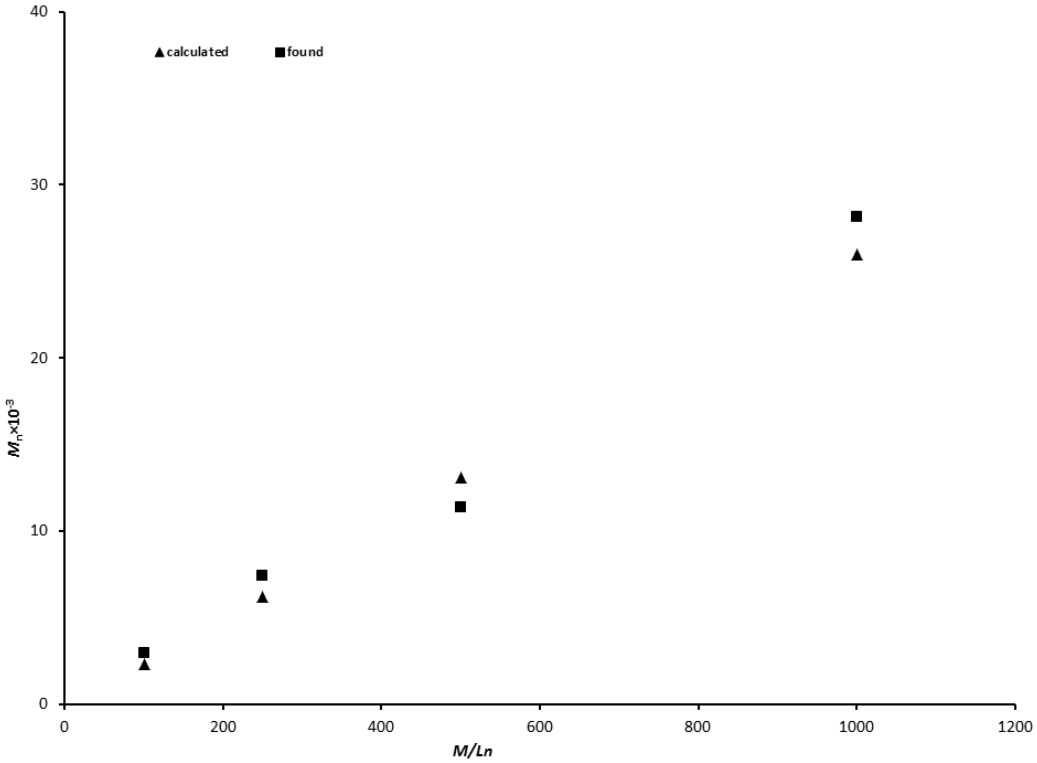

Fig. **S20**. M_n vs $[M]_0/[I]_0$ for ROP of *rac*-LA initiated by **2** in the presence of iPrOH (5 equiv.). Conditions: toluene, 20 °C, $[M]_0$ = 1.0 mol/L.

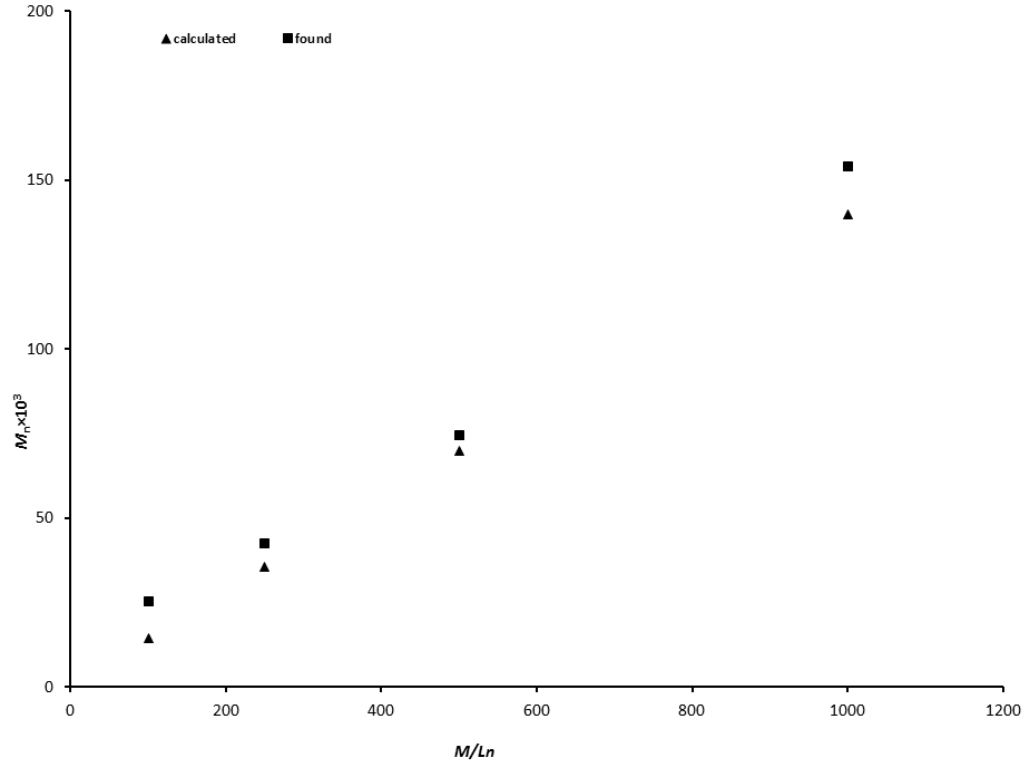

Fig. **S21**. M_n vs $[M]_0/[I]_0$ for ROP of *rac*-LA initiated by **3**. Conditions: toluene, 20 °C, $[M]_0$ = 1.0 mol/L.

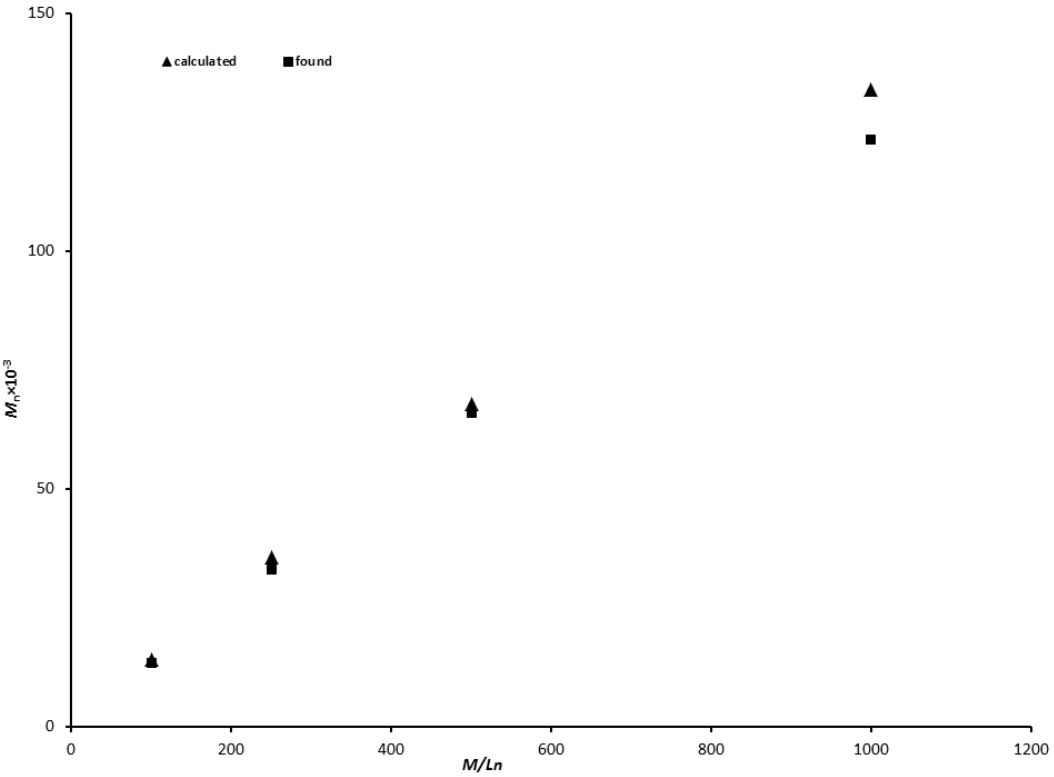

Fig. **S22**. M_n vs $[M]_0/[I]_0$ for ROP of *rac*-LA initiated by **3** in the presence of iPrOH (1 equiv.). Conditions: toluene, 20 °C, $[M]_0$ = 1.0 mol/L.

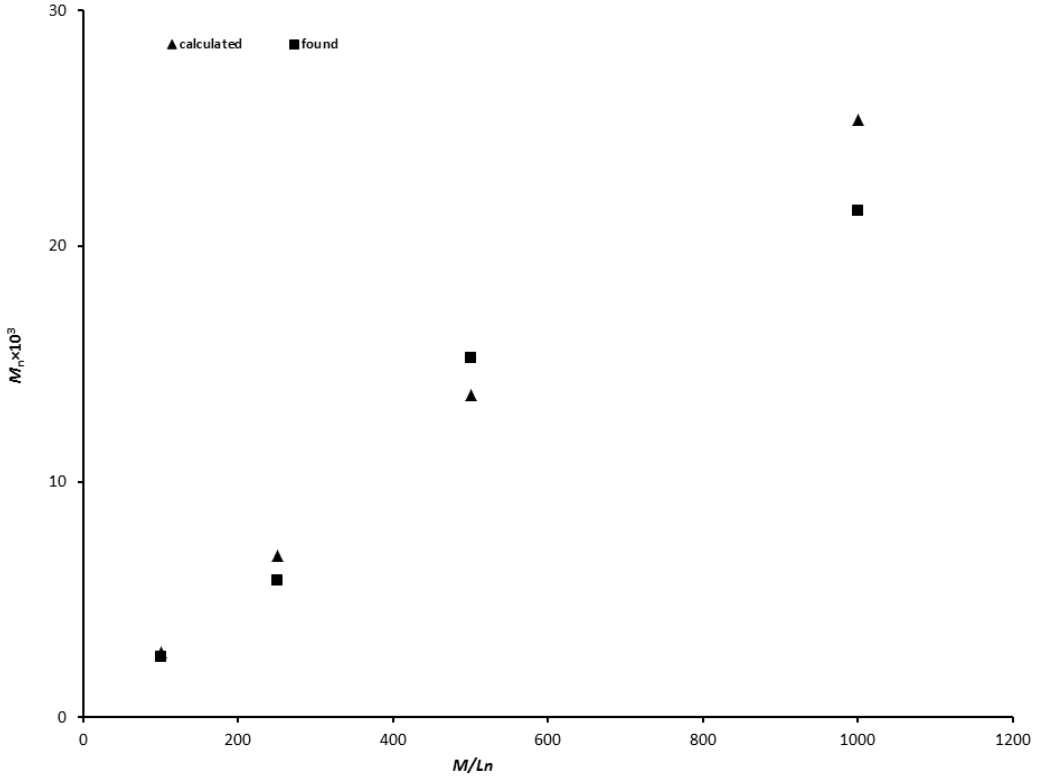

Fig. **S23**. M_n vs $[M]_0/[I]_0$ for ROP of *rac*-LA initiated by **3** in the presence of iPrOH (5 equiv.). Conditions: toluene, 20 °C, $[M]_0$ = 1.0 mol/L.

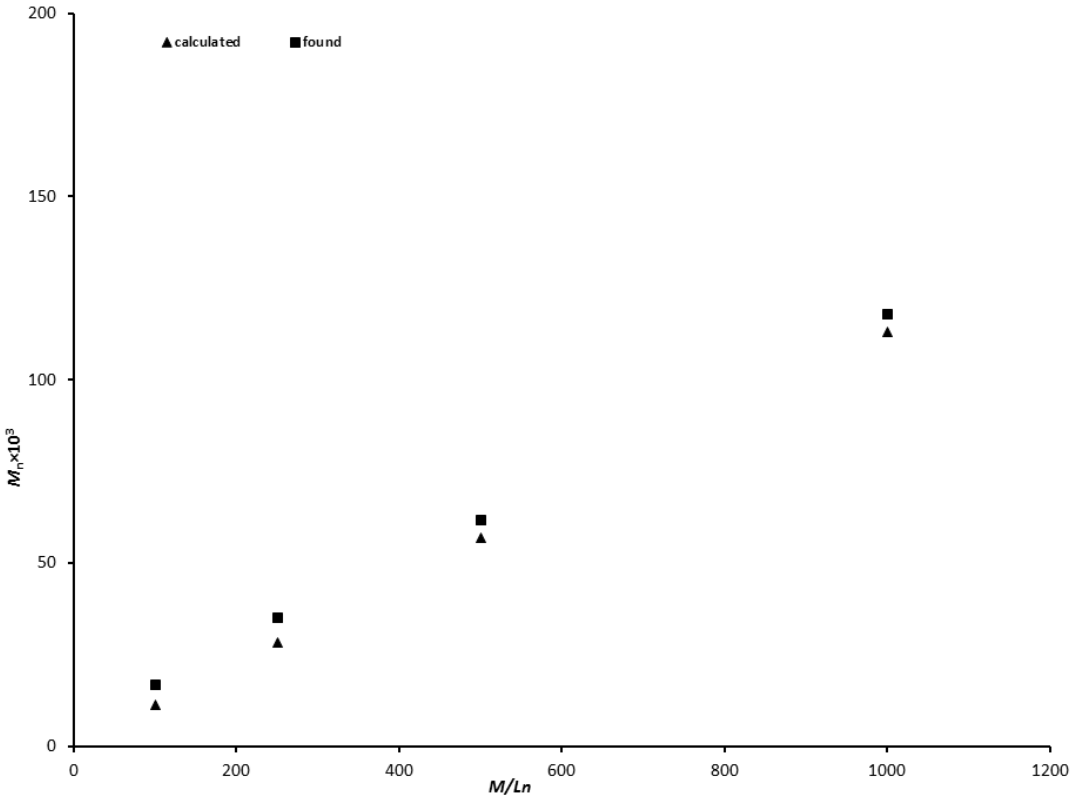

Fig. **S24**. M_n vs $[M]_0/[I]_0$ for ROP of ε-CL initiated by **2**. Conditions: toluene, 20 °C, $[M]_0$ = 1.0 mol/L.

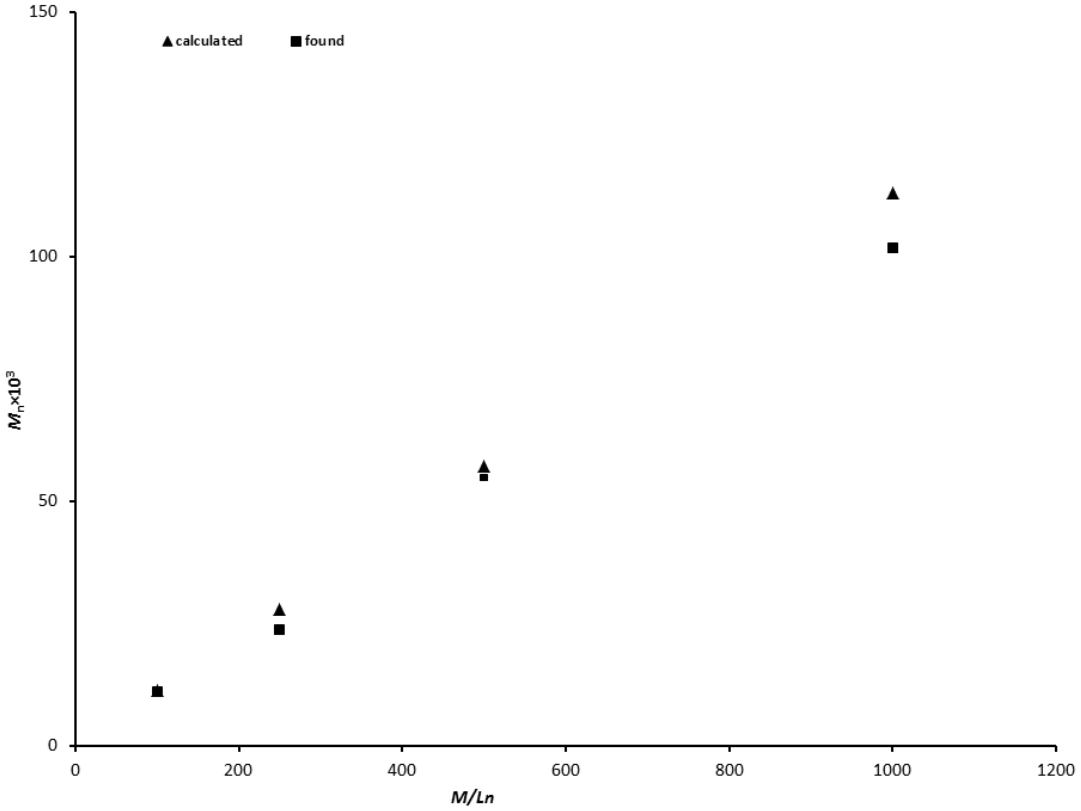

Fig. **S25**. M_n vs $[M]_0/[I]_0$ for ROP of ε-CL initiated by **2** in the presence of iPrOH (1 equiv.). Conditions: toluene, 20 °C, $[M]_0$ = 1.0 mol/L.

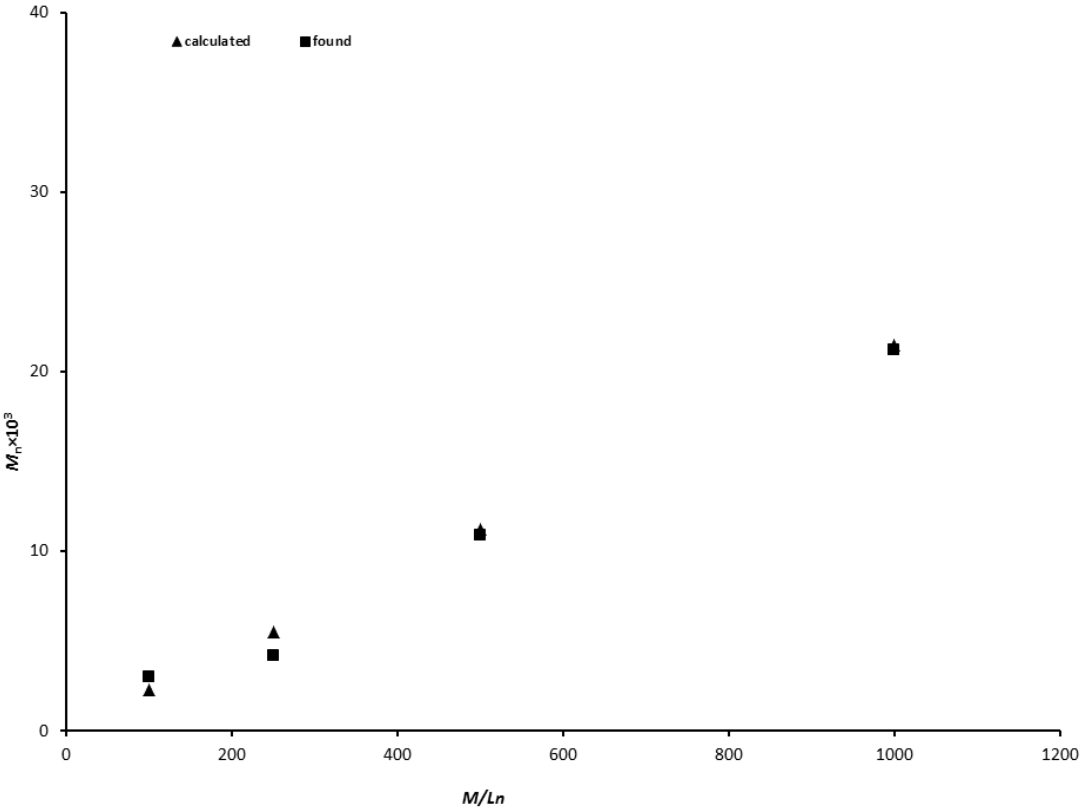

Fig. **S26**. M_n vs $[M]_0/[I]_0$ for ROP of ε-CL initiated by **2** in the presence of iPrOH (5 equiv.). Conditions: toluene, 20 °C, $[M]_0$ = 1.0 mol/L.

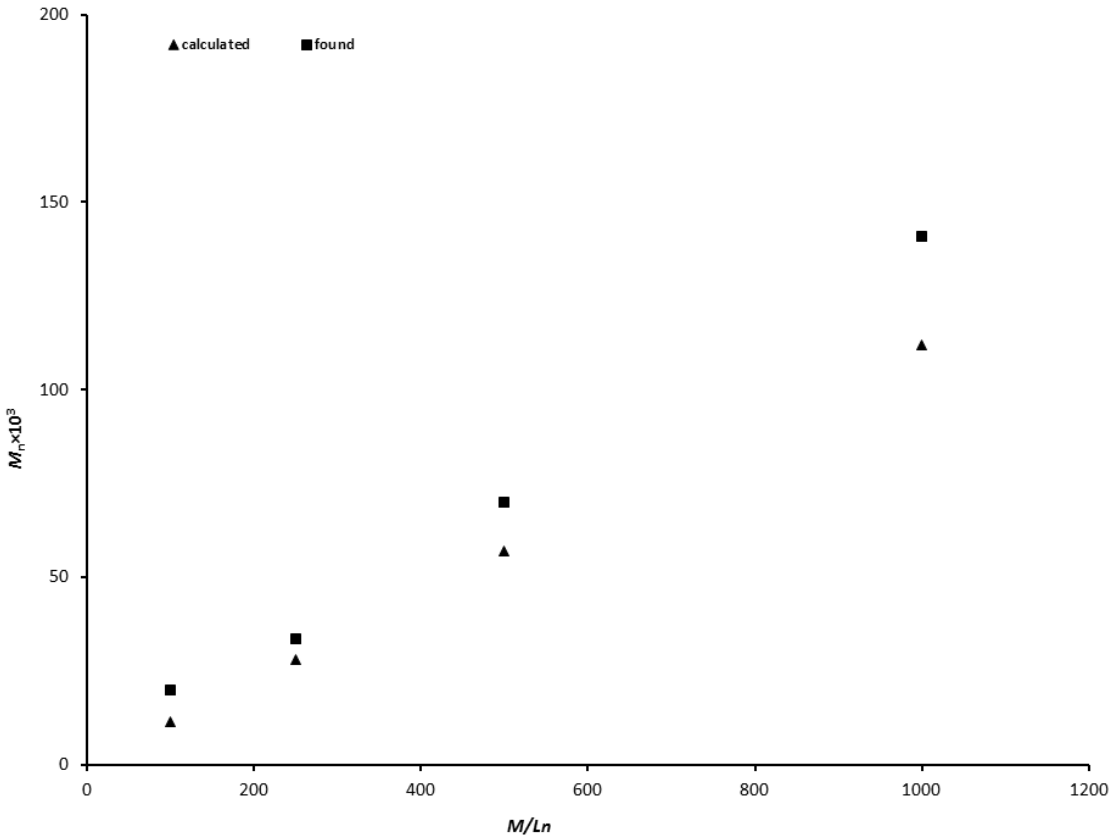

Fig. **S27**. M_n vs $[M]_0/[I]_0$ for ROP of ε-CL initiated by **3**. Conditions: toluene, 20 °C, $[M]_0$ = 1.0 mol/L.

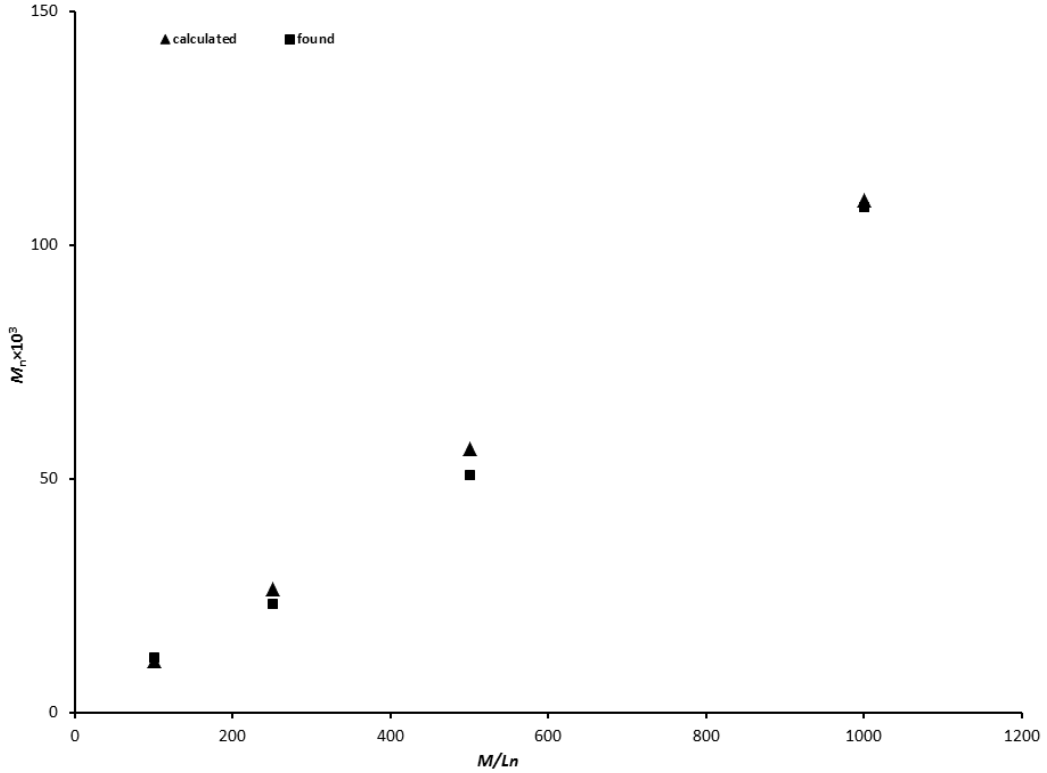

Fig. **S28**. M_n vs $[M]_0/[I]_0$ for ROP of ε-CL initiated by **3** in the presence of iPrOH (1 equiv.). Conditions: toluene, 20 °C, $[M]_0$ = 1.0 mol/L.

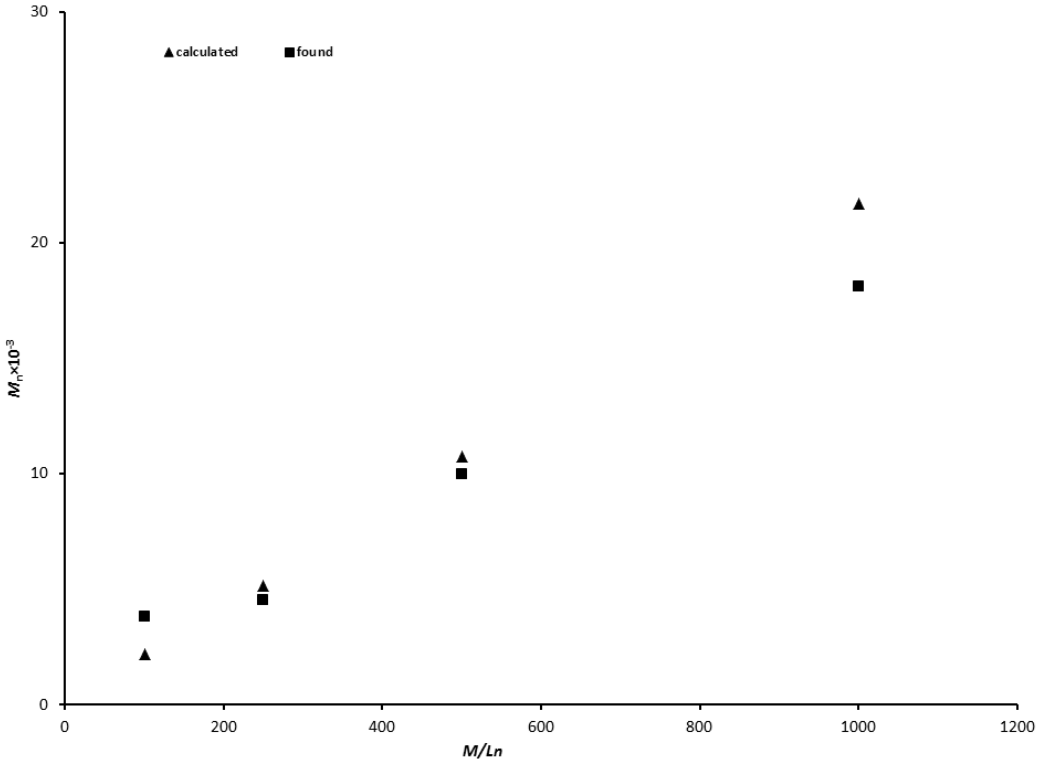

Fig. **S29**. M_n vs $[M]_0/[I]_0$ for ROP of ε-CL initiated by **3** in the presence of iPrOH (5 equiv.). Conditions: toluene, 20 °C, $[M]_0$ = 1.0 mol/L.

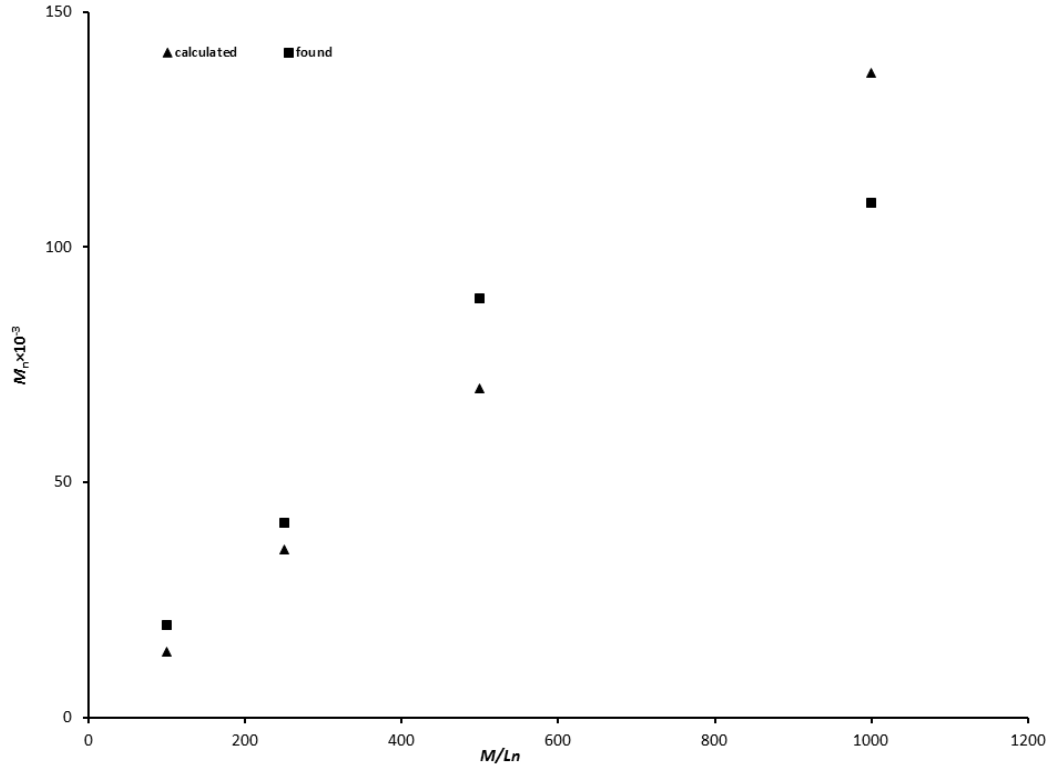

Fig. **S30**. M_n vs $[M]_0/[I]_0$ for ROP of *rac*-LA initiated by **4**. Conditions: toluene, 20 °C, $[M]_0$ = 1.0 mol/L.

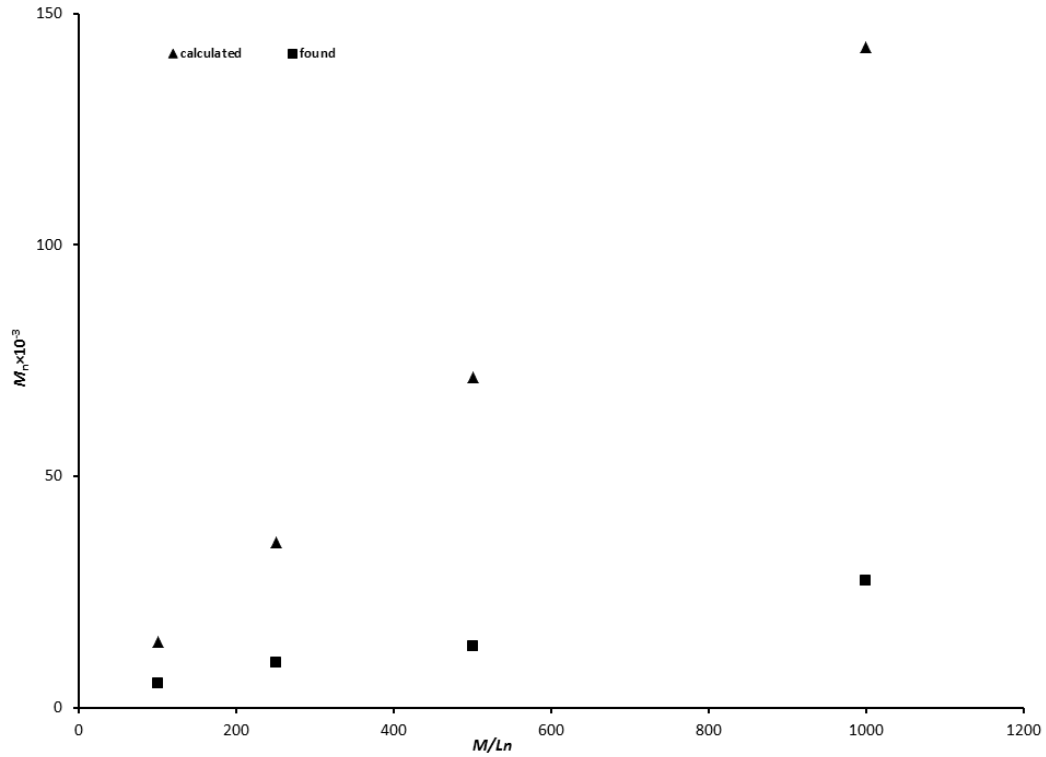

Fig. **S31**. M_n vs $[M]_0/[I]_0$ for ROP of *rac*-LA initiated by **4**. Conditions: T = 120 °C, solvent-free.

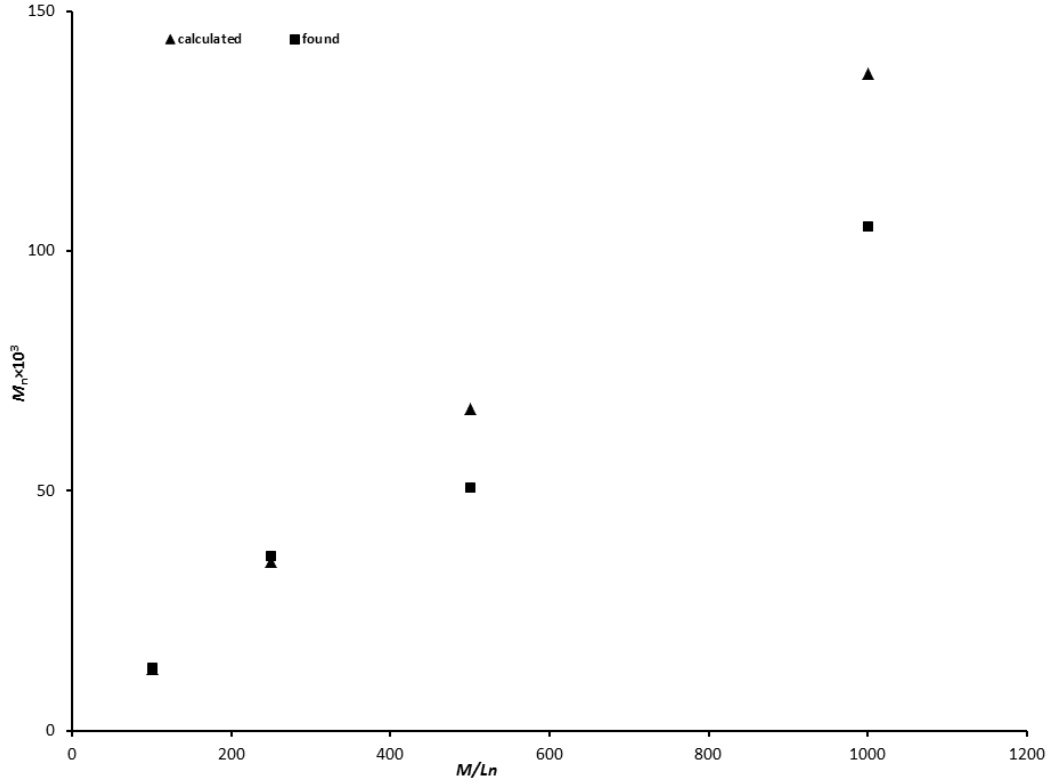

Fig. **S32**. M_n vs $[M]_0/[I]_0$ for ROP of *rac*-LA initiated by **4** in the presence of iPrOH (1 equiv.). Conditions: toluene, 20 °C, $[M]_0$ = 1.0 mol/L.

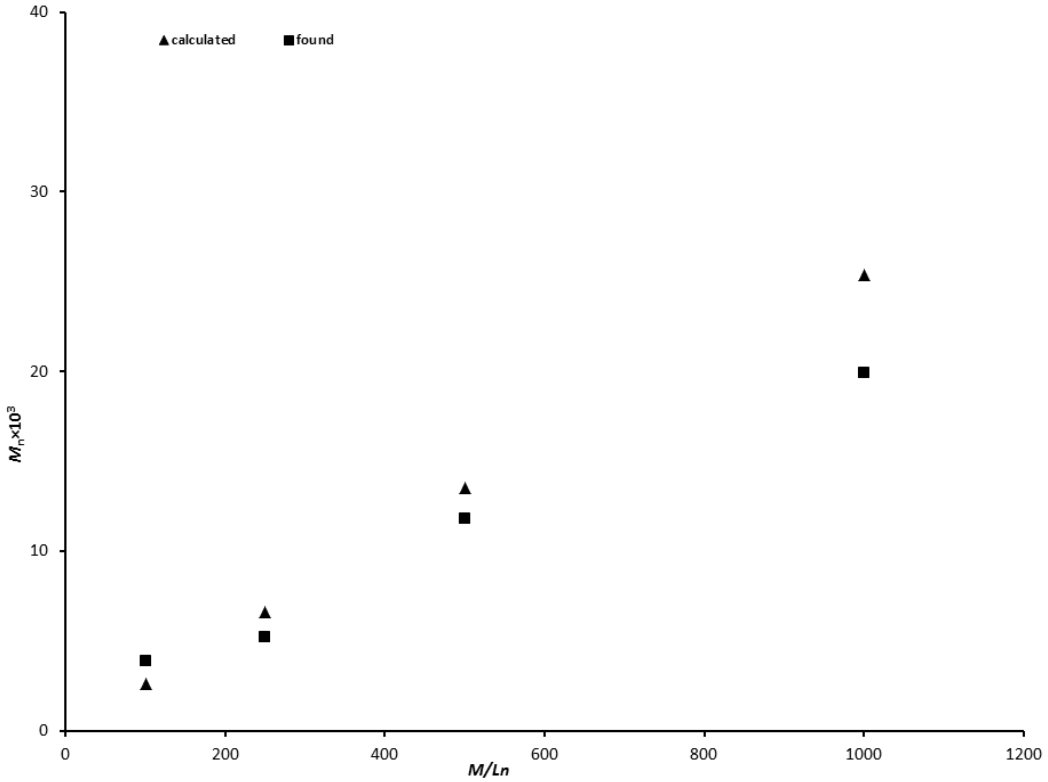

Fig. **S33**. M_n vs $[M]_0/[I]_0$ for ROP of *rac*-LA initiated by **4** in the presence of iPrOH (5 equiv.). Conditions: toluene, 20 °C, $[M]_0$ = 1.0 mol/L.

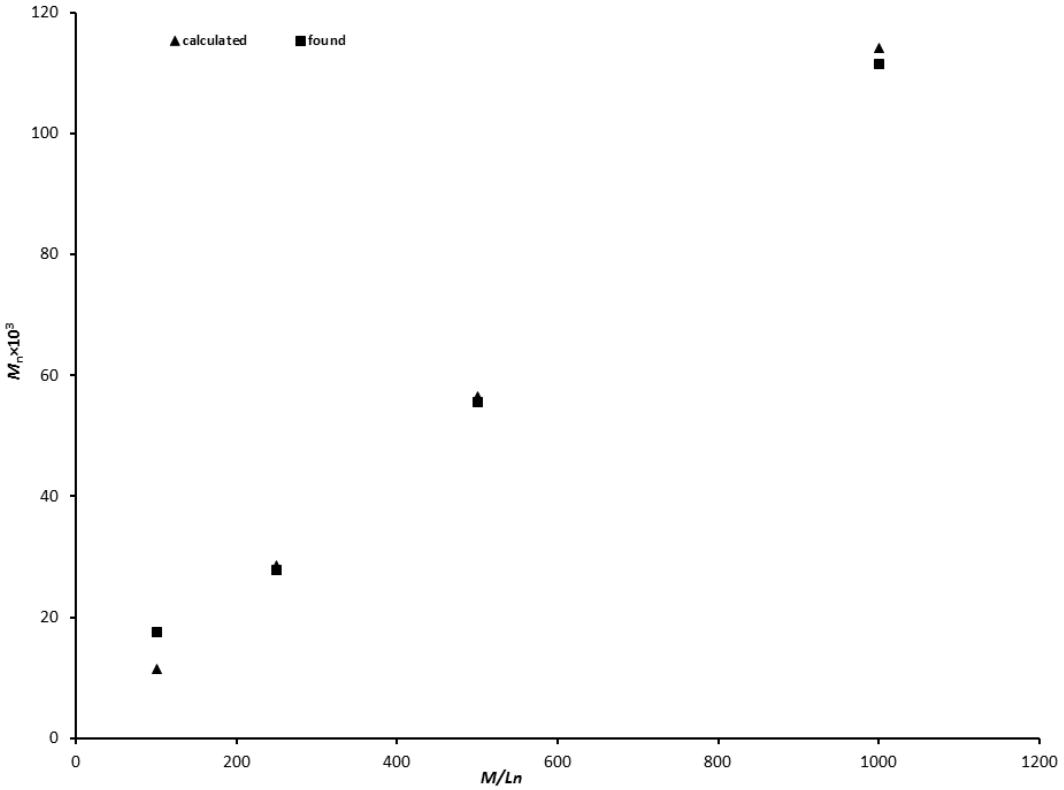

Fig. **S34**. M_n vs $[M]_0/[I]_0$ for ROP of ε-CL initiated by **4**. Conditions: toluene, 20 °C, $[M]_0$ = 1.0 mol/L.

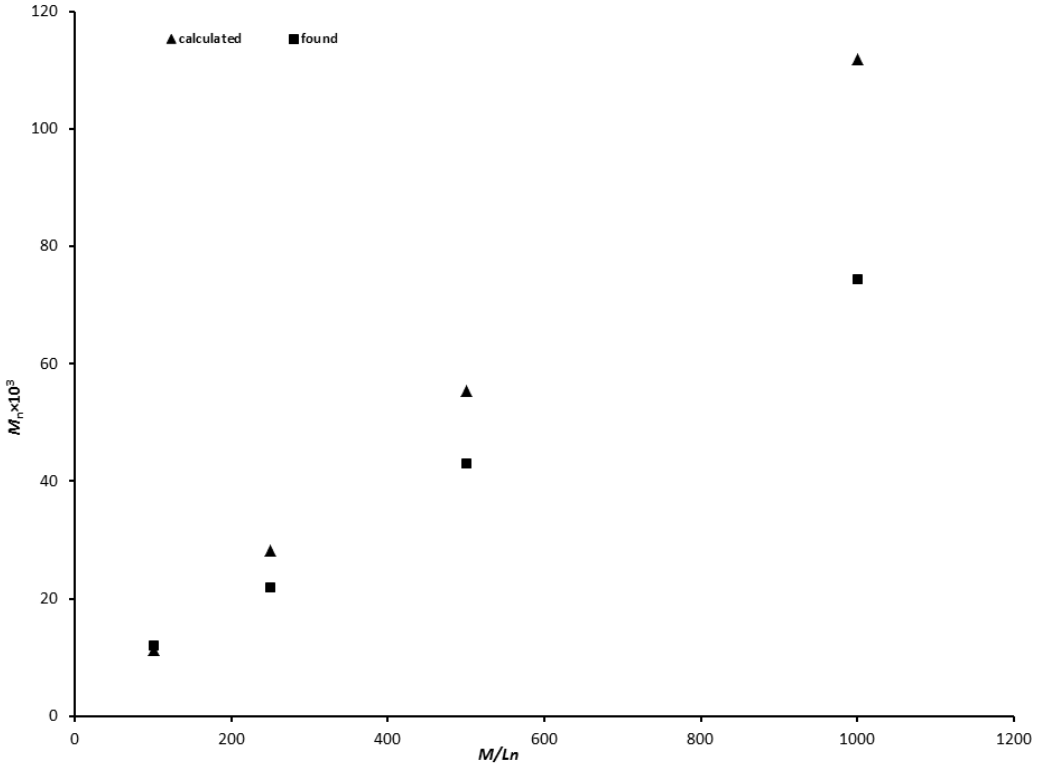

Fig. **S35**. M_n vs $[M]_0/[I]_0$ for ROP of ε-CL initiated by **4** in the presence of iPrOH (1 equiv.). Conditions: toluene, 20 °C, $[M]_0$ = 1.0 mol/L.

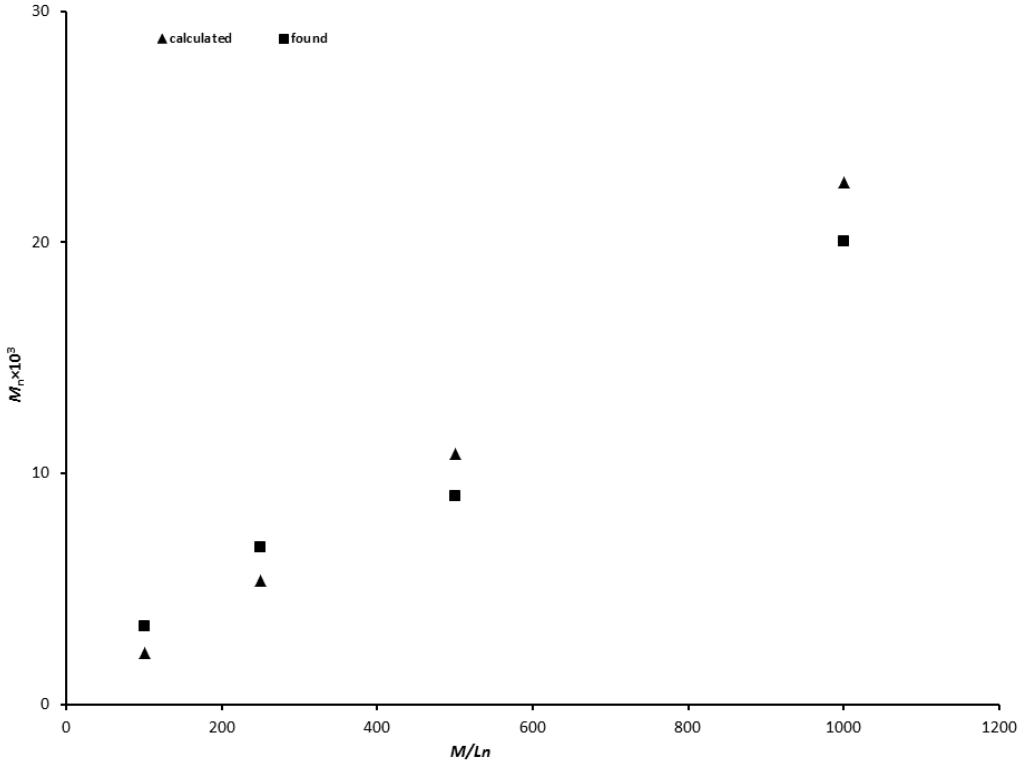

Fig. **S36**. M_n vs $[M]_0/[I]_0$ for ROP of ε-CL initiated by **4** in the presence of iPrOH (5 equiv.). Conditions: toluene, 20 °C, $[M]_0$ = 1.0 mol/L.